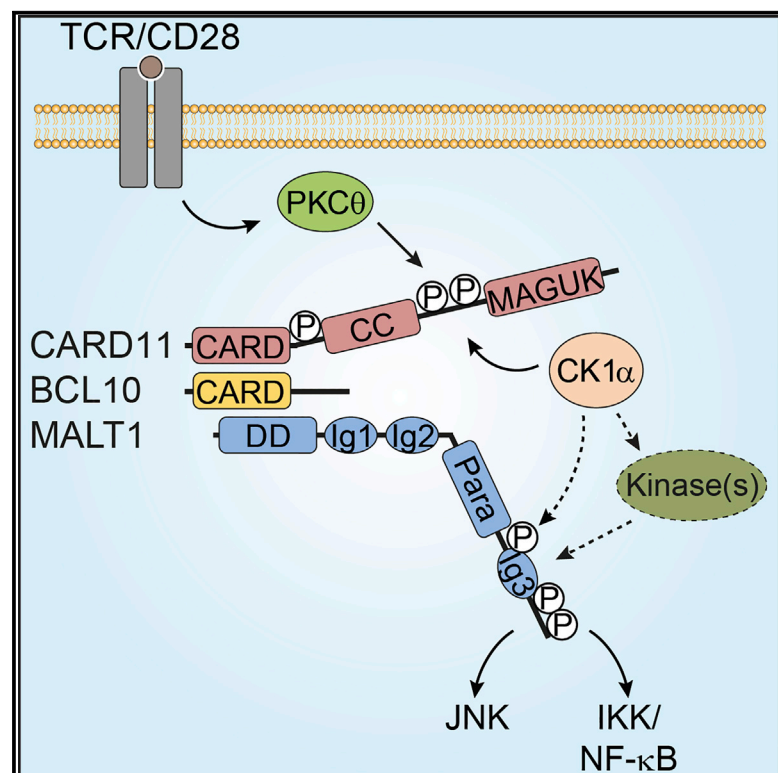


MALT1 Phosphorylation Controls Activation of T Lymphocytes and Survival of ABC-DLBCL Tumor Cells

Graphical Abstract



Authors

Torben Gehring, Tabea Erdmann, Marco Rahm, ..., Stefanie M. Hauck, Georg Lenz, Daniel Krappmann

Correspondence

daniel.krappmann@helmholtz-muenchen.de

In Brief

Gehring et al. identify MALT1 phosphorylation as a process that bridges antigen receptor ligation to downstream signaling pathways in T cells, promotes T lymphocyte activation, and drives survival of B cell lymphoma tumor cells.

Highlights

- Discovery of T cell stimulation-induced MALT1 phosphorylation
- CK1 α activity regulates CBM complex assembly and MALT1 phosphorylation
- MALT1 phosphorylation controls canonical NF- κ B signaling in T cells
- MALT1 phosphorylation promotes survival of ABC-DLBCL tumor cells



MALT1 Phosphorylation Controls Activation of T Lymphocytes and Survival of ABC-DLBCL Tumor Cells

Torben Gehring,¹ Tabea Erdmann,² Marco Rahm,³ Carina Graß,¹ Andrew Flatley,⁴ Thomas J. O'Neill,¹ Simone Woods,¹ Isabel Meininger,^{1,8} Ozge Karayel,⁵ Kerstin Kutzner,¹ Michael Grau,² Hisaaki Shinohara,⁶ Katja Lammens,⁷ Regina Feederle,⁴ Stefanie M. Hauck,³ Georg Lenz,² and Daniel Krappmann^{1,9,*}

¹Research Unit Cellular Signal Integration, Institute of Molecular Toxicology and Pharmacology, Helmholtz-Zentrum München, German Research Center for Environmental Health (GmbH), Ingolstädter Landstraße 1, 85764 Neuherberg, Germany

²Department of Medicine A, Hematology, Oncology and Pneumology, University Hospital Münster, 48149 Münster, Germany

³Research Unit Protein Science, Helmholtz-Zentrum München, German Research Center for Environmental Health (GmbH), Ingolstädter Landstraße 1, 85764 Neuherberg, Germany

⁴Monoclonal Antibody Core Facility and Research Group, Institute for Diabetes and Obesity, Helmholtz-Zentrum München, German Research Center for Environmental Health (GmbH) Ingolstädter Landstraße 1, 85764 Neuherberg, Germany

⁵Department of Proteomics and Signal Transduction, Max-Planck Institute of Biochemistry, Am Klopferspitz 18, 82152 Planegg, Germany

⁶Laboratory for Systems Immunology, Faculty of Pharmaceutical Sciences, Sanyo-Onoda City University, 1-1-1, Daigakudori, Sanyo-onoda City, Yamaguchi 756-0884, Japan

⁷Gene Center, Ludwig-Maximilians University, Feodor-Lynen-Str. 25, 81377 München, Germany

⁸Present address: Center for Infectious Medicine, Department of Medicine, Karolinska Institutet, Stockholm 17177, Sweden

⁹Lead Contact

*Correspondence: daniel.krappmann@helmholtz-muenchen.de
<https://doi.org/10.1016/j.celrep.2019.09.040>

SUMMARY

The CARMA1/CARD11-BCL10-MALT1 (CBM) complex bridges T and B cell antigen receptor (TCR/BCR) ligation to MALT1 protease activation and canonical nuclear factor κ B (NF- κ B) signaling. Using unbiased mass spectrometry, we discover multiple serine phosphorylation sites in the MALT1 C terminus after T cell activation. Phospho-specific antibodies reveal that CBM-associated MALT1 is transiently hyper-phosphorylated upon TCR/CD28 co-stimulation. We identify a dual role for CK1 α as a kinase that is essential for CBM signalosome assembly as well as MALT1 phosphorylation. Although MALT1 phosphorylation is largely dispensable for protease activity, it fosters canonical NF- κ B signaling in Jurkat and murine CD4 T cells. Moreover, constitutive MALT1 phosphorylation promotes survival of activated B cell-type diffuse large B cell lymphoma (ABC-DLBCL) cells addicted to chronic BCR signaling. Thus, MALT1 phosphorylation triggers optimal NF- κ B activation in lymphocytes and survival of lymphoma cells.

INTRODUCTION

Recognition of antigens by cognate antigen receptors expressed on T and B lymphocytes represents the initial step in mounting an adaptive immune response. In lymphoid cells, the CARMA1/CARD11-BCL10-MALT1 (CBM) complex bridges T or B cell antigen receptor (TCR/BCR) proximal signaling to the canonical

nuclear factor κ B (NF- κ B) pathway and c-Jun N-terminal kinase (JNK) activation (Meininger and Krappmann, 2016). Through its scaffolding and proteolytic activities, MALT1 performs a dual role in the CBM complex (Jaworski and Thome, 2016). As an adaptor, MALT1 associates with TRAF6 and potentially other E3 ligases, which catalyze MALT1 poly-ubiquitination on multiple lysine residues in the C terminus, and thereby promotes recruitment of TAK1 and NEMO/IKK β kinases to activate NF- κ B and JNK signaling (Oeckinghaus et al., 2007; Sun et al., 2004). Two alternative splice variants of MALT1 (MALT1A and MALT1B) have been identified that differ in their TRAF6-binding ability, thereby modulating downstream signaling strength and T cell activation (Meininger et al., 2016). The protease function of MALT1 is activated after antigenic stimulation of T cells, requiring mono-ubiquitination on K644 in MALT1A (Coornaert et al., 2008; Pelzer et al., 2013; Rebeaud et al., 2008). MALT1 protease activity does not directly control signaling downstream of the CBM complex (Bornancin et al., 2015; Gewies et al., 2014; Jaworski et al., 2014), but cleavage of MALT1 substrates, such as A20, BCL10, CYLD, HOIL-1, RelB, Regnase-1 (MCP1P1), or Roquin1/2, has been associated with various T cell functions (Coornaert et al., 2008; Haifinger et al., 2011; Jeltsch et al., 2014; Klein et al., 2015; Rebeaud et al., 2008; Staal et al., 2011; Uehata et al., 2013). MALT1 scaffolding and protease activities are also critical for survival of B cells derived from activated B cell-type diffuse large B cell lymphomas (ABC-DLBCLs) that are addicted to chronic BCR signaling or oncogenic CARD11 mutations (Ferch et al., 2009; Haifinger et al., 2009; Ngo et al., 2006).

Several protein kinases regulate the CBM complex by phosphorylating CARD11 and BCL10, thereby positively or negatively affecting T cell activation (Gehring et al., 2018; Meininger and Krappmann, 2016). However, whether MALT1 is



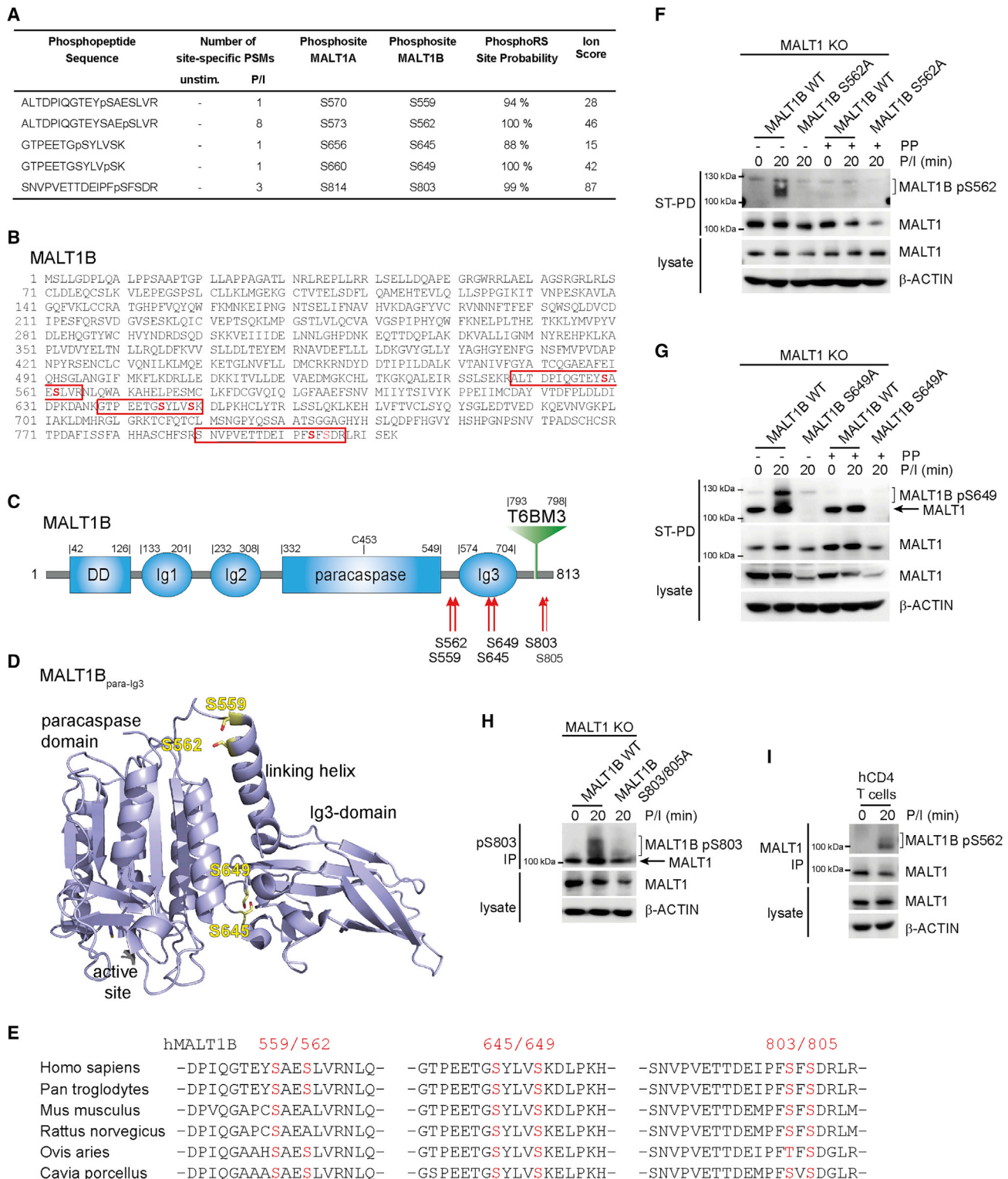


Figure 1. MALT1 Is Phosphorylated on Multiple C-Terminal Serine Residues after T Cell Stimulation
 (A) Overview of identified MALT1 phosphorylation peptides in LC-MS/MS. PSM, peptide-spectrum-match. See also Figures S1A and S1B.
 (B) MALT1B protein sequence with identified phospho-peptides highlighted in red boxes and phospho-serines in red.

(legend continued on next page)

prone to regulatory phosphorylation after T cell stimulation has not been investigated to date. A large-scale proteomic study identified putative phosphorylations in murine MALT1 after BCR ligation, but the sites have not been confirmed or investigated functionally (Satpathy et al., 2015).

Here, we used mass spectrometry and identified multiple C-terminal serine phosphorylations in MALT1 after T cell activation. We demonstrate that MALT1 is hyper-phosphorylated within the CBM complex and that MALT1 phosphorylation regulates TCR/CD28-induced canonical NF- κ B signaling as well as survival of BCR-addicted ABC-DLBCL cells.

RESULTS

MALT1 Hyper-Phosphorylation in Activated T Cells

We performed liquid chromatography coupled to tandem mass spectrometry (LC-MS/MS) to identify phospho-peptides in MALT1 before and after T cell stimulation. To enrich MALT1, we used MALT1 knock out (KO) Jurkat T cells that had been stably reconstituted with human MALT1A C-terminally tagged with a FLAG-StrepII-tag epitope (MALT1A-FS). MALT1A-FS was expressed at endogenous levels and rescued TCR/CD28 signaling and NF- κ B activation in MALT1-deficient Jurkat T cells (Meininger et al., 2016). Strep-Tactin pull-down (ST-PD) led to efficient depletion of MALT1 from the extracts (Figure S1A). Further, we enriched phospho-peptides by titanium dioxide. No MALT1 phospho-peptides were detected in unstimulated Jurkat T cells, but we identified three MALT1 phospho-peptides in phorbol 12-myristate 13-acetate (PMA)/ionomycin (P/I)-treated Jurkat T cells, covering a total of five phosphorylated serine residues that were detected with high confidence (false discovery rate [FDR] < 1%) (Figures 1A and S1B). The putative MALT1 phosphorylation sites correspond to S570, S573, S656, S660, and S814 in human MALT1A or S559, S562, S645, S649, and S803 in human MALT1B (Figures 1A–1C). Interestingly, two identified peptides indicated pairwise phosphorylation at serines in close proximity (S559/S562 and S645/S649 in MALT1B). In the C-terminal phospho-peptide, we also detected a second putative phosphorylation on S805 in MALT1B (S816 in MALT1A) but with lower phosphoRS site probability (Figures 1B and 1C). Nevertheless, the data indicate that the C-terminal phospho-peptide may also contain two adjacent phosphorylation sites on S814/S816 and S803/S805 in MALT1A and MALT1B, respectively. We did not detect dual modified peptides, which we attribute to low abundance and detection thresholds. Because functional analyses were performed with human MALT1B, we subsequently refer to the amino acid position of MALT1B, which lacks exon 7 (aa 309–319) (Meininger et al., 2016).

All phosphorylation sites map to the region of the MALT1 C-terminal in the paracaspase domain (Figure 1C). In the crystal structure of the MALT1_{paracasp-Ig3} fragment, S559 and S562 are located at the start of the linking α -helix that connects the paracaspase and the Ig3 domain (Figure 1D). S645 and S649 are within a connecting loop in the Ig3 domain and near to K633, which is targeted by mono-ubiquitination (Pelzer et al., 2013). S803 and S805 are in the C terminus of MALT1 adjacent to the only functional TRAF6 binding motif (T6BM) in MALT1B, T6BM3 (PVETTD aa 793–798) (Figure 1C) (Meininger et al., 2016; Sun et al., 2004). With the exception of human S562, which is not present in rodent MALT1, the phospho-sites are conserved in mammals (Figure 1E).

To confirm MALT1 phosphorylation and to investigate the regulation, we generated monoclonal antibodies that recognize the phosphorylated serines, which were identified with high confidence (Figure 1A): pS562 (clone 24E9), pS649 (clone 29E12), and pS803 (clone 24A4). Phospho-specific MALT1 detection was assessed by 20 min of P/I stimulation in MALT1 KO Jurkat T cells reconstituted with MALT1B-FS. All three phospho-specific antibodies reacted strongly with slower-migrating, highly modified MALT1B wild type (WT) only after T cell stimulation (Figures 1F–1H). Detection with anti-pS562-, anti-pS649-, and anti-pS803-MALT1 antibodies was severely reduced when phospho-defective MALT1 mutants S562A, S649A, and S803/805A were transduced, respectively. Phosphorylation at S562 and S649 was detected by western blot after Strep-Tactin pull-down (ST-PD) of MALT1B-SF and was completely abolished by phosphatase treatment, confirming detection of phospho-MALT1 (Figures 1F and 1G). MALT1 pS803 was only recognized after anti-pS803-MALT1 immunoprecipitation (IP) followed by anti-MALT1 western blot, indicating that the antibody preferably reacts with pS803 in its native conformation (Figure 1H). Although the anti-pS562-MALT1 antibody exclusively detected hyper-modified and phosphorylated MALT1 (Figure 1F), anti-pS649- and anti-pS803-MALT1 antibodies still retained some activity against unphosphorylated MALT1 (Figures 1G and 1H). In the case of the anti-pS649-MALT1 antibody, detection was phosphatase insensitive but was lost by an S649A exchange, proving that the antibody also detects unmodified S649. In conclusion, we have been able to generate three antibodies that allow monitoring of MALT1 phosphorylation status.

To confirm that MALT1 is also phosphorylated in primary T cells, we stimulated human CD4 T cells purified from donor blood with P/I for 20 min (Figure 1I). With MALT1-IP, we detected phosphorylation at S562 after T cell stimulation, demonstrating that MALT1 is phosphorylated in primary T cells. Thus, by LC-MS/MS and phospho-specific antibodies,

(C) Domain organization of MALT1B protein with positions of phosphorylation sites.

(D) Positions of phospho-serines in the crystal structure of ligand-bound MALT1_{para-Ig3} fragment (PDB: 4I1P).

(E) Evolutionary conservation of identified MALT1 phosphorylation sites in mammals.

(F–H) Generation and validation of antibodies against phosphorylated MALT1B S562 (F), S649 (G), and S803 (H). Phosphorylation specificity was verified with phospho-defective S/A mutant and λ -protein phosphatase (PP) treatment. Phosphorylated MALT1B S803 is detected by the antibody after anti-pS803-IP and MALT1 western blot (WB).

(I) Detection of phosphorylated MALT1B S562 in primary human CD4 T cells isolated from donor blood and stimulated with P/I.

we were able to identify T cell stimulation-dependent phosphorylation of multiple serine residues in the C terminus of MALT1B.

MALT1 Phosphorylation Occurs within the Active CBM Complex

We next used the pMALT1 antibodies to examine T cell stimulation-dependent phosphorylation kinetics of endogenous MALT1 (Figure 2). After stimulation of Jurkat T cells with anti-CD3/CD28 antibodies or P/I, we measured MALT1 phosphorylation as well as CARD11 activation, CBM complex assembly/disassembly, and NF- κ B signaling over a time course up to 8 h (Figures 2A and 2B). Intriguingly, although CARD11 S645 phosphorylation and BCL10-MALT1 recruitment to CARD11 were visible after 2 min of anti-CD3/CD28 or P/I stimulation, MALT1 phosphorylation at the three sites was delayed and peaked after 20–30 min. MALT1 phosphorylation coincided with the onset of I κ B α degradation and the induction of canonical NF- κ B signaling. Although we did not observe significant differences in the initial phosphorylation of the distinct sites, the duration of MALT1 S562 phosphorylation was sustained and still detectable after 1–8 h of stimulation. Thus, MALT1 S562 phosphorylation was also present after CBM-complex disassembly that resulted from BCL10 degradation. In contrast, S649 and S803 phosphorylation rapidly declined after only 30–60 min of stimulation. The data suggested that MALT1 phosphorylation may be involved in CBM downstream effects rather than initial CBM complex assembly.

To test what fraction of MALT1 is phosphorylated in activated T cell, we performed ST-PD of CARD11 KO Jurkat T cells reconstituted with CARD11-FS (Seeholzer et al., 2018). Migration of CARD11-associated MALT1 was severely shifted, which is caused by the multiple mono- and poly-ubiquitinations of CBM-bound MALT1 after T cell stimulation (Figure 2C). In addition, MALT1 S562 and S649 phosphorylations were detected in the CARD11-bound fraction, and phosphorylation was maximal \sim 20 min after P/I treatment. To determine whether proteolytically active MALT1 is phosphorylated, we used the biotin-labeled MALT1 activity-based probe (ABP), which attaches covalently to active MALT1 after stimulation (Eitelhuber et al., 2015). MALT1 ABP precipitated a slower-migrating MALT1 only after P/I stimulation, suggesting that active MALT1 is highly modified, which precisely correlates with the early appearance of mono- and poly-ubiquitinated MALT1 species after 5 min of stimulation (Figure 2D). Indeed, active ABP-coupled MALT1 was also phosphorylated at S562 and S649, and again, MALT1 phosphorylation on both residues was delayed and was first visible after 10 min of P/I treatment, a time point at which MALT1 was already active. As noted earlier, although MALT1 S649 phosphorylation was transient, MALT1 S562 phosphorylation persisted during later time points of MALT1 protease activity. We also monitored MALT1 substrate cleavage and detected CYLD, HOIL-1, and Regnase-1 cleavage from shortly after MALT1 activation and persisting throughout the stimulation time course. Thus, MALT1 phosphorylation takes place within the CBM complex on ubiquitinated and proteolytic active MALT1.

CBM Complex Associated CK1 α Can Act as a MALT1 Kinase

Previous data have demonstrated that the protein kinase CK1 α interacts with CARD11 to regulate the CBM complex upon T cell stimulation (Bidère et al., 2009). CK1 α phosphorylates at “non-primed” sites containing acidic residues in the –3 position or at “primed” sites in which a preceding phosphorylation triggers CK1 α recognition (Venerando et al., 2014). Protein kinase predictions suggest that S562 and S645 in human MALT1B may be putative primed and non-primed substrate sites for CK1 α , respectively (Figure 3A). As suggested earlier, CK1 α binds to CARD11, MALT1, and BCL10 in Jurkat T cells after P/I stimulation (Figure 3B). To clarify which CBM complex members are responsible for CK1 α binding, we determined the association in CARD11, BCL10, and MALT1 KO Jurkat T cells. Absence of any CBM subunit abrogates a complex formation, as evident after BCL10-IP (Figure S2A). In line with the proposed direct recruitment of CK1 α to CARD11 (Bidère et al., 2009), lack of CARD11 abolished CK1 α binding to BCL10 and MALT1 (Figure 3B). However, residual, but severely reduced, CK1 α -CARD11 interaction was detectable in BCL10 or MALT1 KO cells, suggesting that both proteins contribute directly or indirectly to efficient integration of CK1 α into the CBM complex. Next, we determined whether the CK1 α -bound CBM complex contained the MALT1 phosphorylations (Figure 3C). A time-course analysis revealed that CK1 α is recruited to CARD11 and MALT1 within 2 min of P/I stimulation. MALT1 S562 and S649 phosphorylations were detected 10 min after stimulation in the CK1 α -bound CBM complex, demonstrating that CK1 α co-localizes with phosphorylated MALT1 after T cell stimulation.

To investigate the contribution of BCL10-MALT1 to the CK1 α -CARD11 interaction in more detail, we expressed CK1 α -FS and hemagglutinin (HA)-CARD11 alone or together with FLAG-MALT1 and FLAG-BCL10 in HEK293 cells lacking endogenous CARD11 (Figure 3D). Binding of CARD11 to CK1 α was augmented in the presence of BCL10 and MALT1, suggesting that the CBM holo-complex constitutes the optimal platform for CK1 α recruitment. Moreover, we assessed the association of CK1 α -FS to HA-MALT1 (Figure 3E). Although MALT1 did not bind to CK1 α in the absence of BCL10, CK1 α associated with BCL10-MALT1 complexes in the absence of CARD11, and that interaction was not further augmented by CARD11 co-expression or CBM complex formation in HEK293 cells. To verify CARD11-independent interaction of CK1 α with BCL10-MALT1 in Jurkat T cells, we expressed HA-MALT1, FLAG-BCL10, and FLAG-CK1 α in CARD11 KO Jurkat T cells (Figure 3F). Again, HA-MALT1 alone was unable to bind to CK1 α , but BCL10/MALT1 associated with CK1 α , even in the absence of CARD11, implicating BCL10-MALT1 in conferring an additional binding surface for the recruitment of CK1 α to the CBM complex.

To address whether CK1 α can phosphorylate MALT1 at the identified site S562 for which we have generated a highly selective phospho-antibody, we performed *in vitro* kinase assays with recombinant-purified glutathione S-transferase (GST)-MALT1 (aa 325–760) as well as hexa-histidine tag (6xHis)-MALT1-GyrB-HA (aa 334–813) covering the entire C

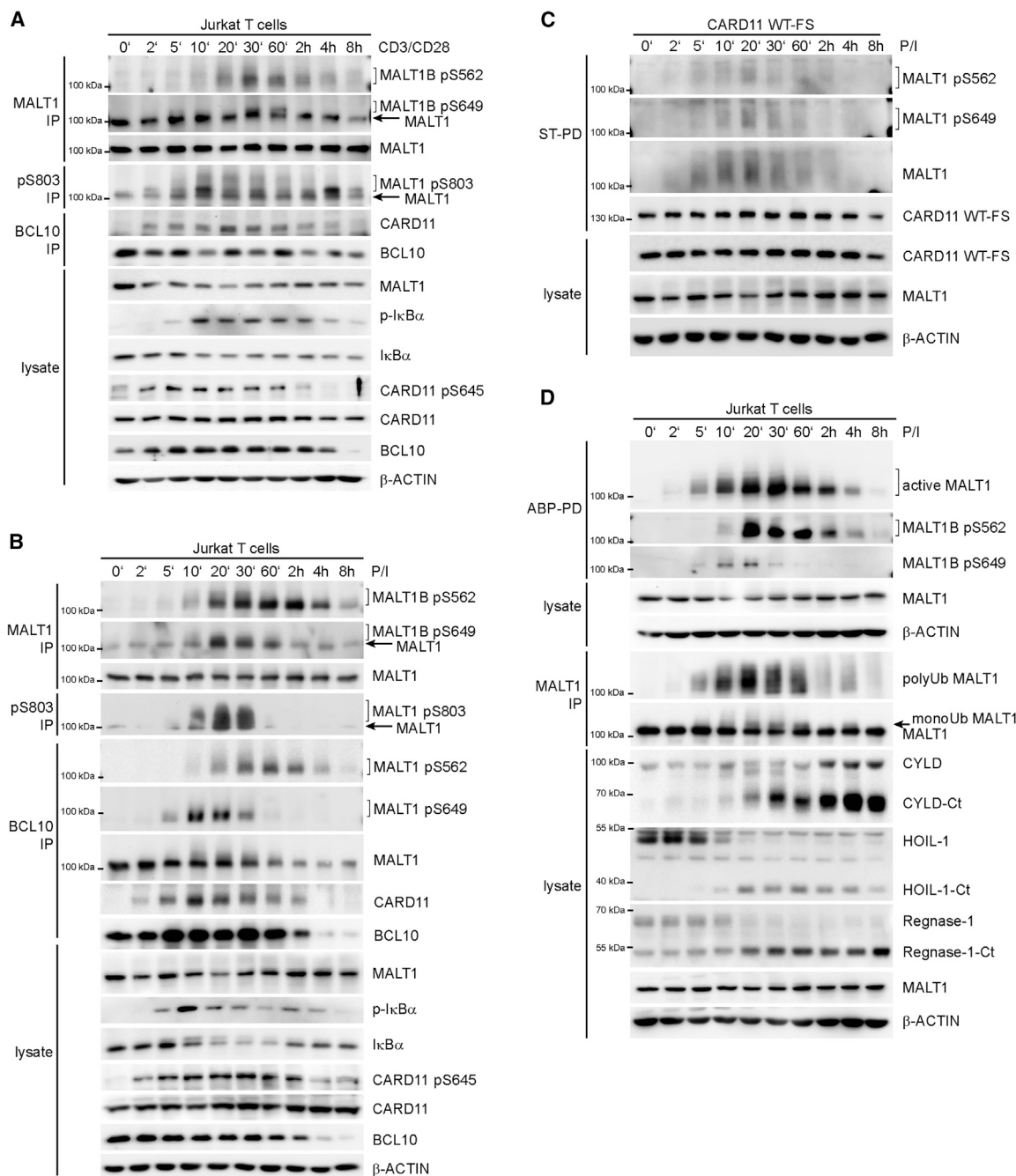


Figure 2. T Cell Stimulation Triggers MALT1 Phosphorylation within the Active CBM Complex

(A and B) Kinetics of MALT1 phosphorylation in Jurkat T cells after CD3/CD28 (A) and P/I (B) stimulation. MALT1 phosphorylation was determined after MALT1-IP (for S562 and S649) or anti-pS803-IP. In parallel, CARD11 S645 phosphorylation, CBM complex formation (BCL10-IP), and IκBα phosphorylation/degradation were determined.

(C) CARD11 association of MALT1 phosphorylated on S562 and S649 after P/I stimulation was detected in CARD11 KO Jurkat T cells reconstituted with CARD11 WT-FS after ST-PD of CARD11.

(D) S562 and S649 phosphorylation of protease active, ubiquitinated MALT1 was detected after MALT1-ABP-PD. In parallel, MALT1 substrate cleavage was detected by WB.

terminus (Figures 3G and S2B). After *in vitro* kinase reactions, recombinant CK1α was able to phosphorylate GST-MALT1 325–760 and His-MALT1 334–813 at serine 562 within the

consensus sequence. Thus, CK1α binds to BCL10/MALT1, associates with p-MALT1 in the CBM complex, and can catalyze *in vitro* phosphorylation on MALT1 at serine 562.

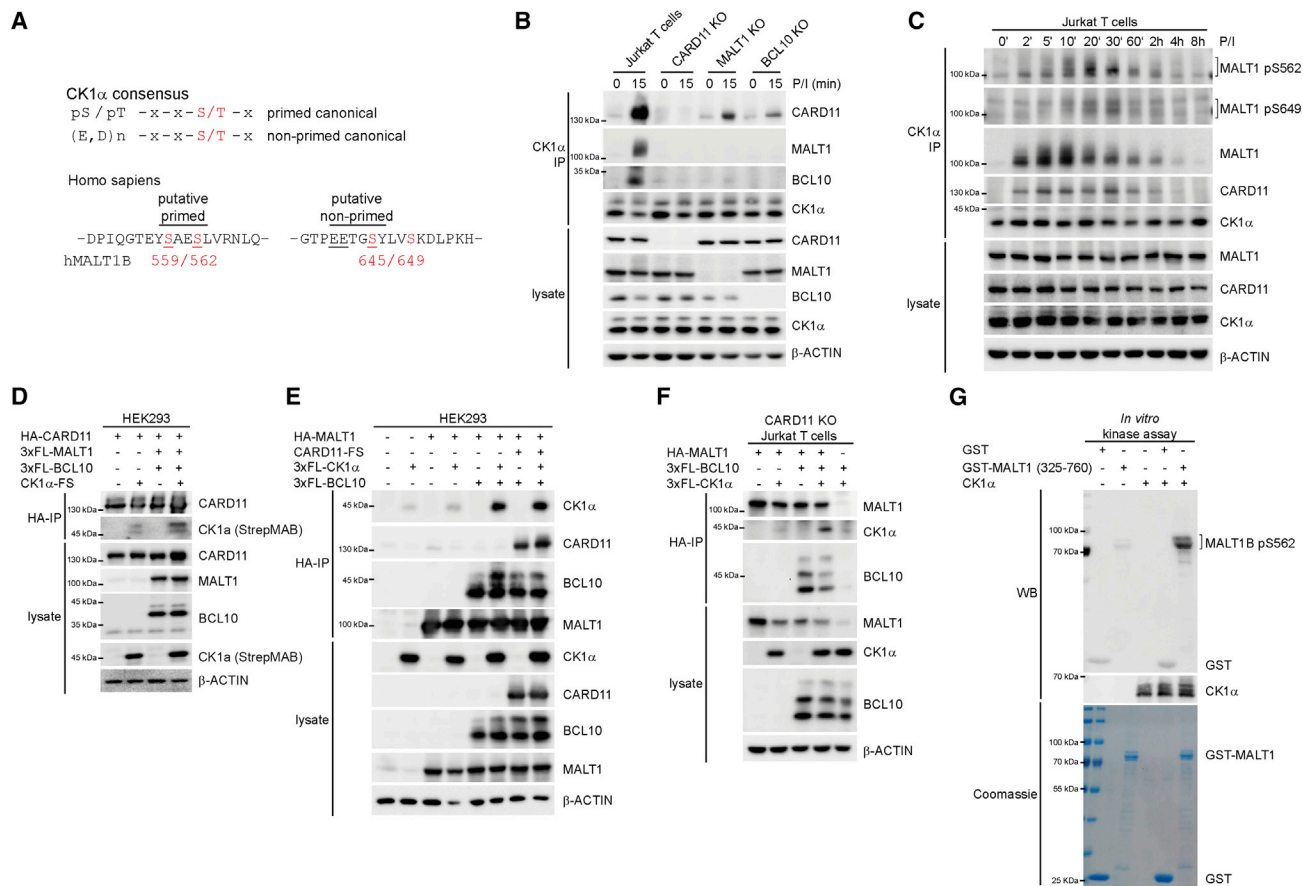


Figure 3. CK1 α Is Recruited to the CBM Holo-Complex and Phosphorylates MALT1 at Serine 562

(A) Consensus sequence of primed canonical or non-primed canonical CK1 α phospho-acceptor sites. Potential primed and non-primed CK1 α phosphorylation sites in human MALT1 are indicated.

(B) Binding of CK1 α to CARD11, MALT1, and BCL10 in parental and respective KO Jurkat T cells after P/I stimulation was determined after CK1 α -IP. See also Figure S2A.

(C) Kinetics of CK1 α association to MALT1 phosphorylated on S562 and S649 was determined by phospho-specific antibodies after CK1 α -IP.

(D) Binding of HA-CARD11 to CK1 α -FS in the absence or presence of 3xFLAG-BCL10 and 3xFLAG-MALT1 in HEK293 cells.

(E) Association between HA-MALT1 and 3xFLAG-CK1 α , either alone or in the presence of only 3xFLAG-BCL10 or 3xFLAG-BCL10 and CARD11-FS in HEK293 cells.

(F) Interaction between HA-MALT1 and 3xFLAG-CK1 α , either alone or in the presence of 3xFLAG-BCL10 in CARD11 KO Jurkat T cells.

(G) *In vitro* CK1 α kinase assay on bacterial GST-MALT1 (aa 325–760) was followed by detection of MALT1 pS562 by WB. See also Figure S2B.

CK1 α Activity Triggers CBM Complex Assembly and Downstream Signaling

CK1 α exerts positive and negative regulatory effects on CBM complex signaling (Bidère et al., 2009). To dissect the role of CK1 α for CBM assembly and downstream function, we generated CK1 α KO Jurkat T cells by using a single-guide RNA (sgRNA) targeting exon3 (Figure S3A). Two independent Jurkat T cell clones were obtained, which had lost CK1 α protein expression because of destructive frameshift mutations in exon 3 (Figures 4A and S3B). CK1 α KO Jurkat T cells were viable and did not exhibit defects in cell growth. To prove that cellular effects are caused by CK1 α KO, we rescued CK1 α KO Jurkat T cell clone 6 with CK1 α WT, kinase-dead D136N or CARD11-binding mutant Y292A (Bidère et al., 2009). CK1 α constructs were homogenously transduced and expressed in CK1 α KO Jurkat T cells, and the slightly altered migration of CK1 α

D136N was due to conformational changes and was not on the level of the mRNA, as revealed by PCR and sequencing (Figures 4B, S3C, and S3D).

We assessed the effects of CK1 α deficiency on CBM downstream signaling in response to T cell stimulation. Indeed, CK1 α deficiency abolished NF- κ B signaling and MALT1 protease activation, as evident from loss of I κ B α phosphorylation/degradation, NF- κ B DNA binding, and MALT1-catalyzed CYLD or HOIL-1 cleavage after anti-CD3/CD28 or P/I stimulation (Figures 4C and S3E). Extracellular signal-regulated kinase (ERK) phosphorylation and protein kinase C theta (PKC θ)-dependent phosphorylation of CARD11 on S645 were normal in CK1 α KO cells, ruling out defective upstream signaling. Moreover, loss of CK1 α did not affect NF- κ B signaling in response to tumor necrosis factor alpha (TNF- α) stimulation (Figure S3F). Reconstitution with CK1 α WT, but not inactive CK1 α D136N,

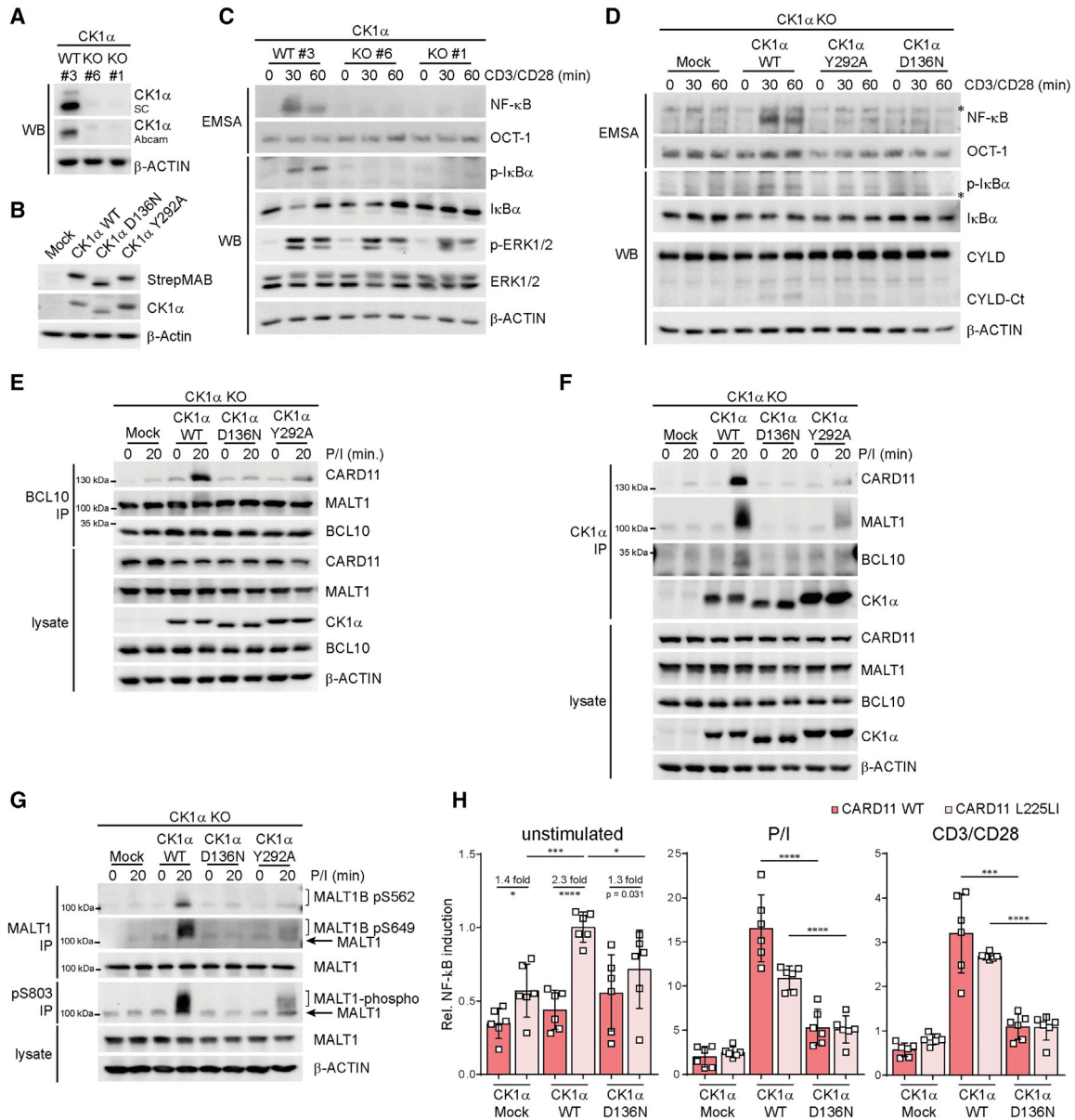


Figure 4. CK1α Kinase Activity and CARD11 Binding Trigger CBM Complex Formation, NF-κB Activation, and MALT1 Phosphorylation

(A) Generation of CK1α KO Jurkat T cells by CRISPR/Cas9. Loss of CK1α was verified by WB. See also Figures S3A and S3B.

(B) Protein expression of CK1α WT, D136N, and Y292A in reconstituted CK1α KO Jurkat T cells was analyzed by WB. See also Figures S3C and S3D.

(C) NF-κB signaling in CK1α KO Jurkat T cells in response to CD3/CD28 stimulation was analyzed by electrophoretic mobility shift assay (EMSA) and WB. See also Figures S3E and S3F.

(D) Effects of CK1α D136N and Y292A mutants on NF-κB signaling and MALT1 activation after CD3/CD28 stimulation was assessed by EMSA and WB. See also Figure S3G. Unspecific bands are marked with asterisk.

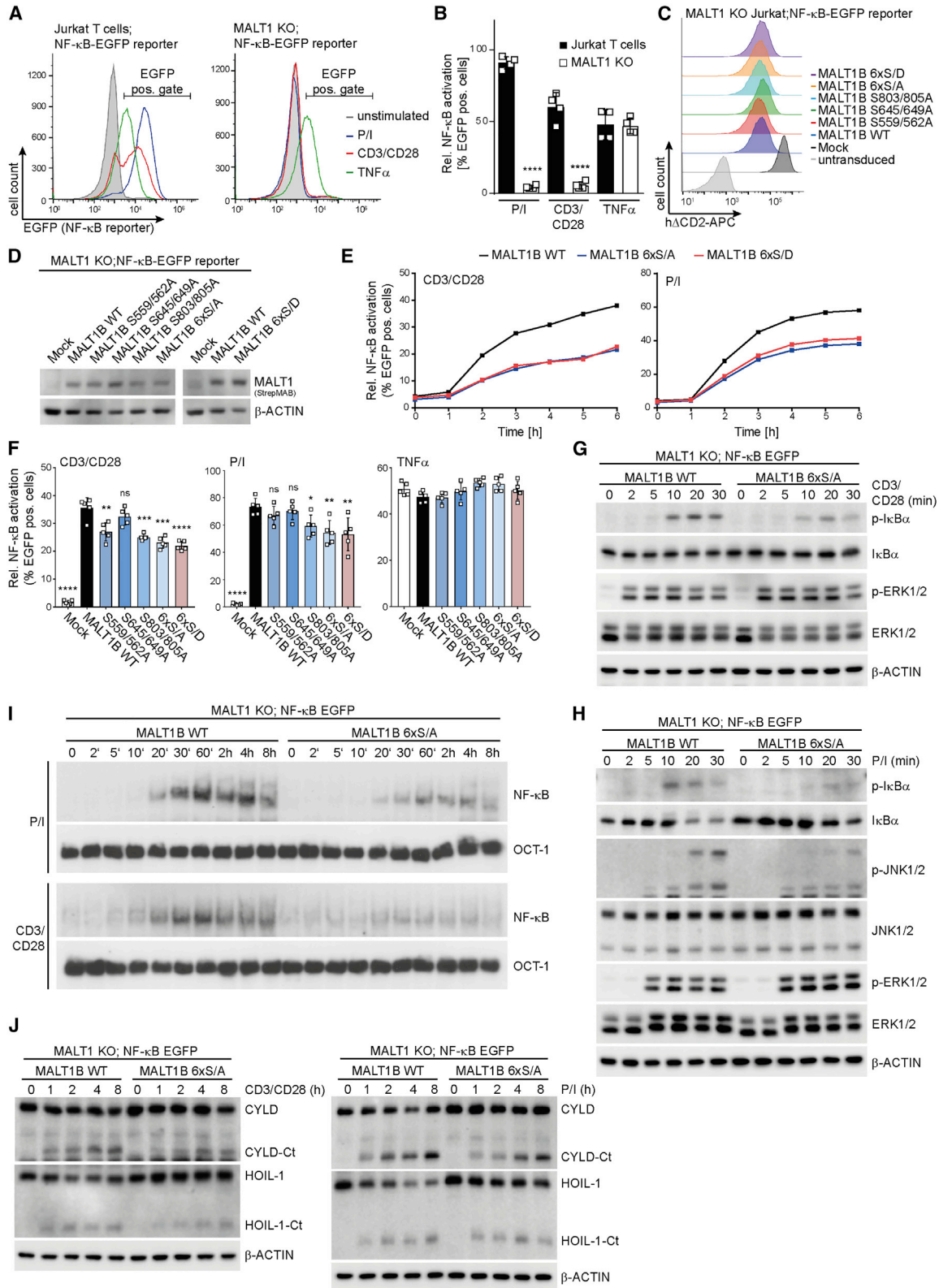
(E) Requirement of CK1α activity and CARD11 binding for CBM complex formation was monitored by BCL10-IP and WB in Jurkat T cells expressing CK1α, D136N, and Y292A mutants. See also Figure S3H.

(F) CK1α recruitment to CARD11, BCL10, and MALT1 was determined by CK1α-IP and WB in CK1α KO Jurkat T cells reconstituted with CK1α WT, D136N, or Y292A mutant.

(G) Analyses of MALT1 phosphorylation on S562, S649, and S803 in Jurkat T cells expressing CK1α WT, D136N, or Y292A. See also Figure S3I.

(H) NF-κB reporter assay after transfection of CARD11 WT or L225LI mutant in CK1α-deficient Jurkat T cells reconstituted with mock, CK1α WT, or D136N mutant. Fold changes in constitutive induction of the NF-κB reporter gene are depicted.

The data represent means ± SD of six biological replicates. *p ≤ 0.05, **p ≤ 0.01, ***p ≤ 0.001, ****p ≤ 0.0001. See also Figure S4.



(legend on next page)

restored NF- κ B signaling and MALT1 protease activation upon T cell stimulation (Figures 4D and S3G). In line with defective signaling, inducible CBM assembly was lost in CK1 α -deficient Jurkat T cells and was rescued by the transduction of CK1 α WT but not the D136N mutants (Figures 4E and S3H). Further, defective CARD11 recruitment by the CK1 α -mutant Y292A severely impaired NF- κ B and MALT1 activation as well as CBM complex formation (Figures 4D, 4E, and S3G). Importantly, neither CK1 α Y292A nor CK1 α D136N was efficiently recruited to CARD11, BCL10, and MALT1 after P/I stimulation, suggesting that the CK1 α -CARD11 interaction, as well as the CK1 α catalytic activity, is required for assembly of the CK1 α -containing CBM complex (Figure 4F). Using phospho-specific MALT1 antibodies, we found that MALT1 phosphorylation on the three serine residues 562, 649, and 803 was lost in the absence of CK1 α (Figures 4G and S3I). Again, although CK1 α WT could rescue MALT1 phosphorylation, MALT1 phosphorylation on all three serines was strongly diminished in the CARD11-binding-defective CK1 α Y292A and absent in the kinase-dead CK1 α D136N (Figure 4G). Thus, CK1 α catalytic activity is essential to initiate CBM complex assembly, which subsequently drives MALT1 protease activation, MALT1 phosphorylation, and downstream signaling.

It has been suggested that CK1 α kinase activity also exerts a negative role in counteracting CBM-triggered T cell activation by phosphorylating S608 in the linker region of CARD11 (Bidère et al., 2009). Indeed, expression of CARD11 S608A in CARD11-deficient JPM50.6 cells was more effective in rescuing NF- κ B activation when compared with CARD11 WT, confirming the negative regulatory effect of CK1 α in the CBM complex (Figures S4A–S4C). Nevertheless, reconstitution of CK1 α KO Jurkat T cells underscores the dominant function of CK1 α catalytic activity as driving CBM complex formation.

Because CK1 α catalytic activity is essential for CBM complex formation, reconstitution experiments are unable to prove whether CK1 α directly catalyzes MALT1 phosphorylation in activated T cells. Nevertheless, to address whether CK1 α kinase activity exercises a catalytic function downstream of CARD11 in the assembled CBM complex, we took advantage of the oncogenic CARD11 L225LI variant, which bypasses the upstream necessity for CK1 α by promoting constitutive CBM complex assembly (Lenz et al., 2008). CK1 α constitutively associates with the CARD11 L225LI-containing CBM complex in the

absence of upstream signaling input (Bognar et al., 2016; Knies et al., 2015). As expected, oncogenic CARD11 L225LI more potently induced NF- κ B reporter gene induction than CARD11 WT in unstimulated CK1 α WT-expressing Jurkat T cells (Figure 4H). However, constitutive NF- κ B induction by CARD11 L225LI was strongly reduced in mock or kinase-dead CK1 α D136N reconstituted CK1 α KO Jurkat T cells, demonstrating that downstream signaling of oncogenic CARD11 is also mediated by CK1 α kinase activity. As expected, NF- κ B activation after P/I or CD3/CD28 stimulation in CARD11 WT and CARD11 L225LI-expressing cells was also strongly diminished in the absence of CK1 α activity. Thus, NF- κ B activation by a constitutively assembled CBM complex still relies on CK1 α activity, strongly arguing for an additional, kinase-dependent downstream function of CK1 α in TCR/CD28 signaling.

MALT1 Phosphorylation Augments Canonical NF- κ B Signaling and T Cell Activation

To determine the contribution of MALT1 phosphorylations for NF- κ B activation, we transduced a viral NF- κ B-EGFP reporter, consisting of EGFP under the control of six NF- κ B sites, into parental or MALT1 KO Jurkat T cells. NF- κ B transcriptional activation was measured by determining EGFP-positive Jurkat T cells using fluorescence-activated cell sorting (FACS) (Figure 5A). Although NF- κ B was induced after P/I, CD3/CD28, or TNF- α stimulation in parental Jurkat T cells, absence of MALT1 abolished EGFP expression in response to P/I or CD3/CD28, but not TNF- α (Figure 5B). We transduced MALT1B WT, pairwise MALT1B phospho-defective mutants (S559/562A, S645/649A, and S803/805A), MALT1B lacking all six phospho-acceptor serines (MALT1B 6xS/A), and the putative phospho-mimetic MALT1B (MALT1B 6xS/D) into MALT1 KO;NF- κ B-EGFP Jurkat T cells (Figure 5C). All MALT1B constructs were expressed at equivalent levels (Figure 5D). We performed a kinetic analysis measuring the number of EGFP-positive Jurkat T cells after CD3/CD28 or P/I stimulation, and decreased expression of the NF- κ B-EGFP reporter was seen at all times between 2 and 6 h of stimulation in MALT1B 6xS/A and 6xS/D compared with the WT (Figure 5E). Quantification of EGFP expression after 5 h of stimulation revealed that combined mutation of all phospho-sites in MALT1B 6xS/A and the double-mutant MALT1B S803/805A were significantly impairing NF- κ B activation in response to P/I or CD3/CD28 (Figure 5F). Decreased NF- κ B activation

Figure 5. C-Terminal MALT1 Phosphorylation Augments NF- κ B Signaling and Activation in Jurkat T Cells

- (A) Induction of NF- κ B-EGFP reporter in parental and MALT1 KO Jurkat T cells as determined by FACS after P/I, anti-CD3/CD28, or TNF- α stimulation.
 (B) Quantification of NF- κ B activation by counting of EGFP-positive cells, see (A), after P/I, anti-CD3/CD28, and TNF- α stimulation. The data represent means \pm SD of four biological replicates. ****p \leq 0.0001.
 (C) Equivalent transduction of MALT1 constructs in MALT1 KO;NF- κ B-EGFP reporter Jurkat T cells was monitored by the surface-marker hCD2 in FACS.
 (D) Protein expression of transduced MALT1 WT and mutants, see (C), was analyzed by WB.
 (E) Number of EGFP-positive cells was determined in MALT1B WT (black), MALT1B 6xS/A (blue), and MALT1B 6xS/D (red) expressing Jurkat T cells after a time course of P/I and CD3/CD28 stimulation by FACS.
 (F) Quantification of NF- κ B activation by EGFP-positive cells in MALT1 KO;NF- κ B-EGFP reporter cells reconstituted with MALT1B WT or phospho-mutants after 5 h of CD3/CD28, P/I, or TNF- α stimulation. The data represent means \pm SD of five biological replicates. *p \leq 0.05, **p \leq 0.01, ***p \leq 0.001, ****p \leq 0.0001.
 (G and H) Effects of combinatory MALT1B 6xS/A mutant on κ B α , JNK, and ERK after CD3/CD28 (G) or P/I (H) stimulation were investigated by WB. See also Figures S5, S6A, and S6B.
 (I) Effects of MALT1B 6xS/A mutant on NF- κ B activation after P/I or CD3/CD28 stimulation was investigated by EMSA. See also Figures S6C–S6E.
 (J) MALT1 substrate cleavage of CYLD and HOIL-1 was determined in MALT1B WT and 6xS/A mutant cells in response to CD3/CD28 and P/I stimulation. See also Figure S6F.

for MALT1B S559/562A was only significant after CD3/CD28 stimulation, whereas MALT1B S645/649A did not show significant effects. MALT1B 6xS/D was unable to rescue NF- κ B activation and thus also acted as a phospho-defective, instead of a phospho-mimetic, mutant. However, replacing a serine with negatively charged aspartic or glutamic acid is often insufficient for acquiring a phospho-mimetic variant, which, for instance, is also observed in the case of I κ B α , where these putative phospho-mimetic residues rendered the NF- κ B inhibitor degradation resistant, just like the phospho-defective serine to alanine mutant (Traenckner et al., 1995; Brockman et al., 1995). MALT1-independent NF- κ B activation in response to TNF- α was unchanged by the MALT1 phospho-mutations (Figure 5F). Thus, MALT1 phosphorylation sites are required for optimal induction of NF- κ B transcriptional responses and C-terminal MALT1 phosphorylations exert combinatorial effects on TCR/CD28-induced NF- κ B activation in Jurkat T cells.

Rescue by the pairwise MALT1 phospho-defective mutants S559/562A, S645/649A, and S803/805A in MALT1 KO Jurkat T cells led to a weak, but consistent, reduction in NF- κ B signaling and activation after CD3/CD28 or P/I stimulation, whereas TNF- α -driven NF- κ B activation was not altered (Figures S5A–S5E). Because we observed combinatorial effects of the phospho-site mutations, we focused on analyzing the biochemical effects of the MALT1 6xS/A and 6xS/D mutants. In line with the decreased NF- κ B reporter-gene activation, P/I- and CD3/CD28-induced I κ B α phosphorylation and degradation were impaired in Jurkat T cells expressing MALT1B 6xS/A (Figures 5G and 5H), leading to severely diminished NF- κ B DNA binding (Figure 5I). In addition, JNK phosphorylation was diminished in the MALT1B phospho-defective mutant 6xS/A, whereas MALT1-independent ERK activation or NF- κ B signaling in response to TNF- α was unaffected (Figures 5G, 5H, and S6A). Similarly, NF- κ B and JNK activation was impeded by expression of MALT1B 6xS/D, confirming that the exchange to aspartic acid resulted in a defective, instead of mimetic, MALT1 variant (Figures S6B and S6C). As expected, C-terminal MALT1 phospho-defective 6xS/A mutations did not interfere with the CBM complex assembly after P/I stimulation (Figure S6D). In addition, MALT1 ubiquitination was not affected in the phospho-defective mutant MALT1B 6xS/A after P/I stimulation, ruling out MALT1 poly-ubiquitination being controlled by phosphorylation (Figures S6D and S6E). MALT1 protease activity and cleavage of CYLD and HOIL-1 by phospho-defective MALT1B 6xS/A was induced in response to T cell stimulation, but slightly less efficiently than MALT1B WT (Figures 5J and S6F). Thus, C-terminal MALT1 phosphorylation is required to couple the CBM complex to optimal downstream signaling.

To corroborate the necessity of MALT1 phosphorylation for activation of primary T cells, we used retroviral transduction to rescue CD4 T cells from MALT1-deficient mice with human MALT1B constructs. Infected CD4 T cells were identified by co-expression of the surface marker Thy1.1, and equivalent expression of MALT1B WT and phospho-mutant proteins was verified by western blot of the sorted cells (Figures 6A and S7A). To determine NF- κ B transcriptional responses in primary T cells, we measured induction of NF- κ B-regulated genes *IL-2*, *TNFAIP3/A20*, and *NFKBIA/I κ B α* in reconstituted MALT1^{-/-}

CD4 T cells after CD3/CD28 stimulation by RT-PCR. The genes were strongly induced in a MALT1-dependent manner after 1–4 h of TCR/CD28 stimulation (Figures 6B and S7B). Similar to what was found for NF- κ B reporter activation in Jurkat T cells, phospho-defective MALT1B mutants were impaired in upregulating the target genes, and again, the combined mutation of all six phosphorylation sites in 6xS/A most severely affected the induction of all three genes (Figures 6B and S7B).

We used single-cell FACS to investigate the effects of MALT1 phospho-mutants on NF- κ B signaling and IL-2 protein expression in CD4 T cells. P/I stimulation for 20 min did not induce I κ B α degradation in untransduced MALT1-deficient, Thy1.1-negative or mock-infected, Thy1.1-positive CD4 T cells (Figures 7C and S7C). In contrast, reconstitution of MALT1B WT rescued stimulus-dependent I κ B α degradation (Figure 6C). I κ B α degradation was still detectable in the MALT1B phospho-defective mutants S559/562A, S645/649A, and S803/805A, but was significantly less pronounced than in MALT1B WT (Figures 6C and 6D). Combined mutation of all six serine residues in MALT1B 6xS/A most severely attenuated I κ B α degradation in CD4 T cells. Furthermore, we measured intracellular IL-2 expression by FACS in reconstituted CD4 T cells after anti-CD3/CD28 or P/I stimulation to confirm that defective MALT1 phosphorylation prevents optimal T cell activation (Figures 6E–6H). Although expression of MALT1B WT rescued induction of IL-2 in MALT1^{-/-} CD4 T cells, upregulation of IL-2 was significantly impaired in the phospho-defective mutants, and the strongest effects were observed by mutating all phospho-sites in MALT1B 6xS/A. Taken together, MALT1 phosphorylation in the C terminus channels the CBM complex to canonical NF- κ B signaling and gene induction in Jurkat and CD4 T cells after TCR/CD28 co-stimulation.

Phosphorylation of the MALT1 C Terminus Contributes to Survival Signaling in ABC-DLBCL Cells

As part of the CBM complex, MALT1 is essential for controlling NF- κ B survival signaling in ABC-DLBCL cells (Ngo et al., 2006). We, therefore, tested whether MALT1 is prone to chronic phosphorylation in ABC-DLBCL cell lines by using anti-pS562-MALT1, the antibody that most effectively and selectively recognizes phosphorylated MALT1 in human cells (see Figure 2). After MALT1-IP, we detected phosphorylation of MALT1 on S562 in all four ABC-DLBCL cell lines (HBL1, TMD8, OCI-Ly3, and U2932) even in the absence of stimulation (Figure 7A). We did not detect constitutive MALT1 phosphorylation on S562 in the germinal center B cell-like (GCB) DLBCL cell lines BJAB, SUDHL4, and SUDHL6, but phosphorylation in SUDHL4 and SUDHL6 was induced by P/I stimulation (Figure 7B). To determine whether MALT1 phosphorylation in HBL1 and TMD8 cells, carrying upstream mutations in the BCR-adaptor CD79B, relies on upstream signaling, we treated those cells with Bruton tyrosine kinase (BTK) inhibitor ibrutinib (Figure 7C). Phosphorylation of MALT1 was sensitive to BTK inhibitor treatment, revealing that it is dependent on chronic upstream BCR signaling. In contrast, MALT1 phosphorylation in OCI-Ly3 cells, carrying an oncogenic variant of CARD11, was more resistant to ibrutinib treatment than the HBL1 and TMD8 cells were (Figure 7C). Furthermore, expression of oncogenic CARD11 L225LI in HBL1 cells, which

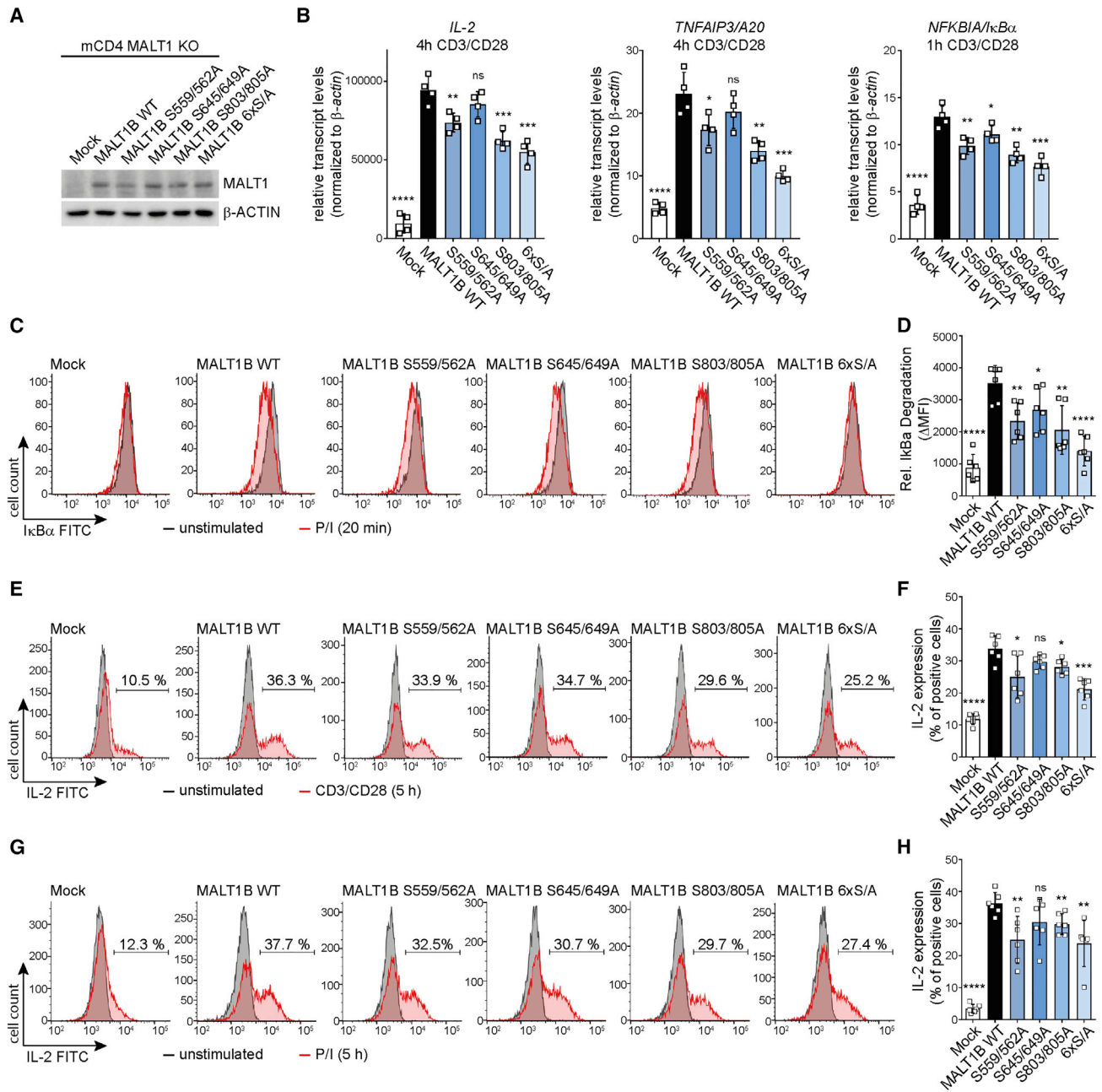


Figure 6. MALT1 Phosphorylation Enhances NF-κB Signaling and IL-2 Expression in CD4 T Cells

(A) Expression of MALT1 WT and S/A mutants was analyzed by WB. See also Figure S7A.

(B) Analyses of induction of *IL-2*, *TNFAIP3/A20*, and *NFKBIA/IκBα* in MALT1 KO CD4 T cells reconstituted with MALT1B WT or phospho-defective S/A mutants after CD3/CD28 stimulation. Transcript levels were normalized to mRNA levels of *β-actin*. The data represent means ± SD of four biological replicates. **p* < 0.05, ***p* < 0.01, ****p* ≤ 0.001, *****p* < 0.0001. See also Figure S7B.

(C and D) Single-cell analyses of IκBα protein levels before and after P/I stimulation were analyzed in MALT1B WT and S/A mutant reconstituted CD4 T cells by intracellular staining and FACS (C). Median fluorescence intensity (MFI) of IκBα-fluorescein isothiocyanate (FITC) was quantified, and induction of IκBα degradation was determined by forming the difference in MFI of unstimulated to stimulated cells. Relative IκBα degradation between MALT1B WT and S/A mutant cells was compared and statistically analyzed (D). The data represent means ± SD of six biological replicates. **p* < 0.05, ***p* < 0.01, *****p* < 0.0001. See also Figure S7C.

(E–H) Single-cell analyses of IL-2 production before and after CD3/CD28 (E and F) or P/I (G and H) stimulation was analyzed in MALT1B WT and S/A mutant-reconstituted CD4 T cells by intracellular staining and FACS (E and G). IL-2 induction was determined by the percentage of IL-2-expressing cells in unstimulated and stimulated cells. Relative IL-2 induction between MALT1B WT and S/A mutant cells was compared and analyzed statistically (F and H). **p* < 0.05, ***p* < 0.01, ****p* < 0.001, *****p* < 0.0001.

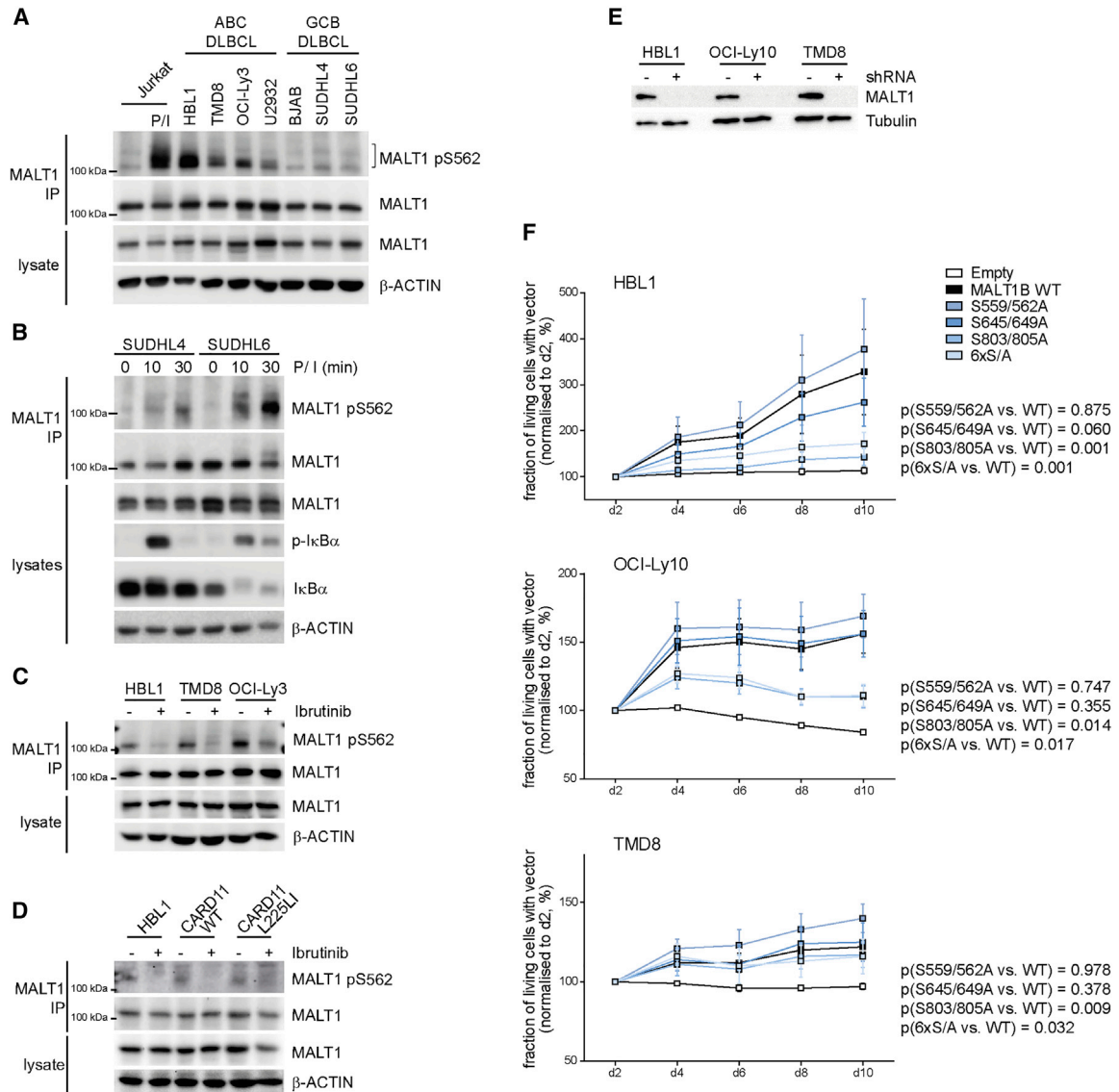


Figure 7. Phosphorylation in the MALT1 C Terminus Contributes to Survival Signaling in ABC-DLBCL Cells

(A) MALT1B S562 phosphorylation was determined after MALT1-IP and WB in four ABC and three GCB DLBCL cell lines, as depicted.
 (B) MALT1B S562 phosphorylation was determined after MALT1-IP and WB, following P/I stimulation in GCB DLBCL cell lines SUDHL4 and SUDHL6.
 (C) ABC-DLBCL cells HBL1, TMD8, and OCI-Ly3 were treated with the BTK inhibitor ibrutinib (20 nM, 18 h), and MALT1B S562 phosphorylation was assessed after MALT1-IP and WB.
 (D) ABC-DLBCL cell line HBL1, transduced with mock, CARD11 WT, or CARD11 L225LI, was treated with the BTK inhibitor ibrutinib (20 nM, 18 h), and MALT1B S562 phosphorylation was assessed after MALT1-IP and WB.
 (E) Knockdown of endogenous MALT1 in rescue experiments was determined by WB 2 days after transduction of shRNA in HBL1, TMD8, and OCI-Ly10 cells.
 (F) HBL1, TMD8, and OCI-Ly10 were transduced with MALT1 shRNA and then infected with mock, MALT1B WT, or mutant constructs. EGFP-positive cells in mock, MALT1 WT, and mutants at days 2–10 after transduction were measured. Time series depict ratios of cells expressing GFP compared with the subset of all living cells, normalized to day 2. Error bars depict SEMs (\pm SEM) over four biological replicates for each time point and vector. Statistical analyses was performed as described in [Method Details](#); p values are given for one-tailed growth comparisons over all time points for S/A mutant cells versus MALT1B WT cells.

reduces ibrutinib toxicity (Nagel et al., 2015), impaired the decrease of MALT1 S562 phosphorylation in response to BTK inhibition (Figure 7D). Thus, the constitutive CBM complex assembly, as a result of chronic BCR signaling or oncogenic CARD11 mutations, induces S562 phosphorylation of MALT1 in ABC-DLBCL cells.

MALT1 silencing induces toxicity to ABC-DLBCL cells (Ngo et al., 2006). To assess the functional consequences of constitutive C-terminal MALT1 phosphorylation in ABC-DLBCL cells, we downregulated endogenous MALT1 by retroviral short hairpin RNA (shRNA) knock down in the ABC-DLBCL cell lines HBL1, OCI-Ly10, and TMD8 (Figure 7E). Subsequently, cells

were reconstituted with MALT1B WT or the MALT1B phospho-defective mutants S559/562A, S645/649A, S803/805A, or combined 6xS/A. EGFP served as a marker to follow the fate of the transduced tumor cells (Figure 7F). As expected, silencing of MALT1 led to growth arrest in all ABC-DLBCL cell lines, which was restored upon ectopic expression of MALT1B WT. The MALT1B phospho-mutant S559/562A and S645/649A did not significantly affect cell growth of ABC-DLBCL cells. However, the MALT1 S803/805A mutant, as well as the combined MALT1 6xS/A, significantly impaired the ability of MALT1 to rescue growth of the three ABC-DLBCL cell lines (Figure 7F). Thus, phosphorylation at the C terminus of MALT1 exerts a positive role that is essential for the survival of BCR-addicted ABC-DLBCL cells.

DISCUSSION

In an unbiased mass spectrometry approach, we have identified several C-terminal phosphorylation sites on MALT1 in activated Jurkat T cells. MALT1 is prone to multiple covalent modifications upon acute TCR/CD28 co-stimulation in T lymphocytes or chronic BCR signaling in ABC-DLBCL cells (Bidère et al., 2009; Ferch et al., 2009; Oeckinghaus et al., 2007), and so far, MALT1 modifications have been primarily attributed to regulatory K63-linked poly-ubiquitination on multiple C-terminal lysines and mono-ubiquitination on K644 in MALT1A, driving NF- κ B and MALT1 protease activation, respectively (Düwel et al., 2009; Oeckinghaus et al., 2007; Pelzer et al., 2013). To these ubiquitin-linkages, we now add stimulus-dependent phosphorylation as a regulatory process that controls MALT1 function. By a MALT1-directed MS approach we identified six C-terminal phosphorylation sites in activated T cells; of which, two sites (S649 and S803) have also been found in a global phospho-proteome approach after IgM-crosslinking in a murine B cell line (Satpathy et al., 2015), indicating comparable regulation in T and B cells. Interestingly, MALT1 modifications are confined to the flexible C terminus, which protrudes from the densely packed BCL10/MALT1 core filaments that are connected by a CARD-DD interface (Schlauderer et al., 2018). Thus, the MALT1 C terminus, encompassing the paracaspase domain, Ig3 domain, and TRAF6 binding motifs represents the “outer” surface of the CBM complex, which is responsible for connecting to various downstream signaling mediators and MALT1 substrates. In line with that, a highly dynamic modification network involving poly-/mono-ubiquitination and phosphorylation controls MALT1 scaffolding and protease activity upon T cell stimulation.

MALT1 is phosphorylated with similar kinetics at S562, S649, and S803 after T cell stimulation, suggesting that they may act in a concerted manner in augmenting NF- κ B signaling. Indeed, co-immunoprecipitations studies reveal that pS562 and pS649 are detected on active MALT1 within the CBM complex, suggesting that not the majority of MALT1 is prone to phosphorylation, but only the fraction engaged in signaling. Similarly, although mutation of all six phospho-acceptor sites caused the strongest effects on NF- κ B activation, pairwise mutations were not as severe. However, in addition, the pairwise MALT1B mutants provided a consistent picture because the strongest effects were observed with the very C-terminal mutation S803/805A, whereas

S559/562A or S645/659A displayed milder or no effects on NF- κ B activation, respectively. The combined action of MALT1 phosphorylation also indicates that the lack of serine 562 in rodents may not have a detrimental effect on signal propagation. In general, weaker CD3/CD28 induction more severely relied on intact phosphorylation sites compared with strong P/I stimulation, suggesting that MALT1 phosphorylation may facilitate conversion of a weak antigen-receptor stimulus into a robust T cell response. Interestingly, the viability of NF- κ B-addicted ABC-DLBCL lymphoma cells also relies on MALT1 phosphorylation, and again, the 6xS/A or the most C-terminal S803/805A caused the strongest effects on MALT1-dependent ABC-DLBCL cell survival. The identification of MALT1 phosphorylation represents a step forward in the understanding how the multi-protein CARD11-BCL10-MALT1 complex controls signaling in physiological and pathological settings (Phelan et al., 2018; Qiao et al., 2013).

We have been able to identify CK1 α as a protein kinase that can bind to BCL10-MALT1 and at least *in vitro* directly phosphorylate MALT1 on S562. We confirmed the association of CK1 α with the CBM complex and demonstrated that it functions as a negative regulator in TCR-induced NF- κ B activation by phosphorylating the putative CK1 α phospho-acceptor S608 in CARD11 (Bidère et al., 2009). However, by reconstituting CK1 α KO Jurkat T cells, we clearly demonstrate that the main role of CK1 α kinase activity is to foster CBM formation and, thus, to promote T cell activation. Initial CARD11 linker phosphorylation at S645 catalyzed by PKC θ is unchanged in the absence of CK1 α , indicating that CK1 α is not involved in upstream events (Shinohara et al., 2007; Sommer et al., 2005). Notably, in the case of WNT signaling, CK1 α functions as a primed kinase that catalyzes the hierarchical multi-site phosphorylation of the adenomatous polyposis coli (APC) protein after initial GSK3 β phosphorylation. In contrast, CK1 α can act as a priming kinase for GSK3 β on β -catenin (Cesaro and Pinna, 2015; Cruciat, 2014). GSK3 β was also found to associate with the CBM complex and to promote NF- κ B signaling in T and B cells (Abd-Allah et al., 2018; Bogner et al., 2016). It is tempting to speculate that, after the initial priming phosphorylation in CARD11 by PKC θ or other potential initiator kinases, CK1 α contributes to CARD11 hyper-phosphorylation and thereby induces the conformational changes that provide accessibility of the CARD-domain for BCL10-MALT recruitment (Chan et al., 2013). Such positive feedback of CK1 α with other protein kinases on the level of CARD11 could also support the reported switch-like mechanism for IKK/NF- κ B activation by the CBM signaling complex (Shinohara et al., 2014). Importantly, CK1 α also exerts a positive effect in the context of oncogenic CARD11 L225LI that assembles independently from upstream signaling, indicating that CK1 α also regulates CARD11 downstream events. MALT1 is not phosphorylated on serines 562, 645, and 803 in CK1 α kinase dead cells, but the concomitant loss of CBM complex formation precludes a demonstration of CK1 α as a direct MALT1 kinase in T cells. Moreover, despite the fact that CK1 α can phosphorylate S562 *in vitro*, it is unlikely that it directly catalyzes all phosphorylations in the MALT1 C terminus. Nevertheless, as with CARD11 hyper-phosphorylation, it is possible that CK1 α is either primed by initial phosphorylation or alternatively, primes phosphorylation by other protein

kinases to induce switch-like activation of MALT1 downstream signaling.

MALT1 phosphorylation takes place within the assembled CBM complex on ubiquitin-modified MALT1, implying that ubiquitination precedes phosphorylation. Active MALT1 is ubiquitinated and phosphorylated, but in contrast to mutation of the mono-ubiquitin acceptor site K644 in MALT1A, MALT1 protease activation and substrate cleavage is not severely altered in the phospho-defective mutants (Pelzer et al., 2013). Phosphorylations may have some effects on the conformational rearrangements in the MALT1 Ig3 domain that are required to activate MALT1 protease (Wiesmann et al., 2012), but MALT1 phosphorylation primarily controls MALT1 scaffolding function and optimal NF- κ B and JNK signaling in activated T cells. The exact mechanisms needs to be resolved, but it seems likely that MALT1 C-terminal phosphorylations induce conformational changes that promote downstream signaling, e.g., by facilitating the recruitment of additional factors. It has been suggested that I κ B α directly associates with MALT1 after TCR/CD28 co-ligation in a CK1 α -dependent manner (Carvalho et al., 2010), suggesting that coordinated recruitment of the IKK and I κ B α /NF- κ B complexes promotes efficient activation of canonical NF- κ B signaling. Different modifications on MALT1 may cooperate in driving optimal NF- κ B activation, which may allow for an “all-or-nothing” activation above and prevent a potentially harmful activation below a certain signaling threshold. With the available tools, we have not been able to detect a potentially very transient CBM holo-complex that contains NEMO/IKK β as well as I κ B α /NF- κ B, but future structural work elucidating the periphery of the BCL10-MALT1 filaments will certainly help to unravel how ubiquitination and phosphorylation cooperate in the regulation of CBM downstream signaling.

STAR★METHODS

Detailed methods are provided in the online version of this paper and include the following:

- KEY RESOURCES TABLE
- LEAD CONTACT AND MATERIALS AVAILABILITY
- EXPERIMENTAL MODELS AND SUBJECT DETAILS
 - Cell culture
 - Isolation and cultivation of primary murine CD4 T cells
 - Isolation and cultivation of primary human CD4 T cells
- METHOD DETAILS
 - Generation of CK1 α -deficient Jurkat T cells
 - Lentiviral transduction of Jurkat T cells
 - Retroviral reconstitution of CD4 T cells from MALT1 KO mice
 - Retroviral transduction of MALT1 shRNA and rescue in DLBCL
 - Transfection in HEK293 cells
 - Electroporation of CARD11 KO Jurkat T cells
 - Stimulation of Jurkat T cells and primary human CD4 T cells
 - Stimulation of primary murine CD4 T cells
 - Generation and analyses of NF- κ B-EGFP reporter Jurkat T cells

- Staining of surface molecules
- Intracellular cytokine staining
- Quantitative analyses of NF- κ B target gene induction
- Preparation of whole cell lysates
- Co-immunoprecipitation (co-IP) and Strep-Tactin pull-down (ST-PD)
- Detection of active MALT1 using MALT1 activity based probes
- Generation of anti-MALT1 S562, S649 and S803 phospho-specific antibodies
- Western Blotting
- Electrophoretic mobility shift assay
- NF- κ B luciferase and EGFP reporter assays
- Production and purification of recombinant proteins
- Generation of MALT1 protein using the baculoviral expression system
- *In vitro* kinase assay
- Sample preparation for phospho-peptide analyses of MALT1
- LC-MS/MS data acquisition
- Mass spectrometric raw data processing and analyses
- QUANTIFICATION AND STATISTICAL ANALYSES
- DATA AND CODE AVAILABILITY

SUPPLEMENTAL INFORMATION

Supplemental Information can be found online at <https://doi.org/10.1016/j.celrep.2019.09.040>.

ACKNOWLEDGMENTS

We thank Katrin Demski and Samyuktha Suresh for excellent technical support. We are grateful to Z.J. Chen for providing the MALT1-GyrB construct. This work was supported by the Deutsche Forschungsgemeinschaft CRC1054/A04 and CRC1054/B02 to D.K. and K.L., respectively, and Deutsche Forschungsgemeinschaft CRC1335/P07 and the Deutsche Krebsstiftung award 70112622 to D.K.

AUTHOR CONTRIBUTIONS

T.G. designed and performed most of experiments. T.E., C.G., T.J.O., S.W., I.M., and K.K. performed or contributed to specific experiments. M.R., A.F., O.K., M.G., H.S., K.L., R.F., S.M.H., and G.L. helped with conducting specific experiments, generated and provided important reagents, gave advice, and designed and supervised the experiments. D.K. conceived the project and designed the experiments. T.G. and D.K. wrote the paper. All authors have read and approved the manuscript.

DECLARATION OF INTERESTS

The authors declare no competing interest.

Received: November 30, 2018

Revised: June 24, 2019

Accepted: September 12, 2019

Published: October 22, 2019

REFERENCES

Abd-Allah, A., Voogdt, C., Krappmann, D., Möller, P., and Marienfeld, R.B. (2018). GSK3 β modulates NF- κ B activation and RelB degradation through site-specific phosphorylation of BCL10. *Sci. Rep.* 8, 1352.

- Bidère, N., Ngo, V.N., Lee, J., Collins, C., Zheng, L., Wan, F., Davis, R.E., Lenz, G., Anderson, D.E., Arnould, D., et al. (2009). Casein kinase 1 α governs antigen-receptor-induced NF- κ B activation and human lymphoma cell survival. *Nature* 458, 92–96.
- Bognar, M.K., Vincendeau, M., Erdmann, T., Seeholzer, T., Grau, M., Linneemann, J.R., Ruland, J., Scheel, C.H., Lenz, P., Ott, G., et al. (2016). Oncogenic CARMA1 couples NF- κ B and β -catenin signaling in diffuse large B-cell lymphomas. *Oncogene* 35, 4269–4281.
- Bornancin, F., Renner, F., Touil, R., Sic, H., Kolb, Y., Touil-Allaoui, I., Rush, J.S., Smith, P.A., Bigaud, M., Junker-Walker, U., et al. (2015). Deficiency of MALT1 paracaspase activity results in unbalanced regulatory and effector T and B cell responses leading to multiorgan inflammation. *J. Immunol.* 194, 3723–3734.
- Brockman, J.A., Scherer, D.C., McKinsey, T.A., Hall, S.M., Qi, X., Lee, W.Y., and Ballard, D.W. (1995). Coupling of a signal response domain in I kappa B alpha to multiple pathways for NF- κ B activation. *Mol. Cell. Biol.* 15, 2809–2818.
- Carvalho, G., Le Guellec, A., Demian, C., Vazquez, A., Gavard, J., and Bidère, N. (2010). Interplay between BCL10, MALT1 and I κ B α during T-cell-receptor-mediated NF κ B activation. *J. Cell Sci.* 123, 2375–2380.
- Cesaro, L., and Pinna, L.A. (2015). The generation of phosphoserine stretches in phosphoproteins: mechanism and significance. *Mol. Biosyst.* 11, 2666–2679.
- Chan, W., Schaffer, T.B., and Pomerantz, J.L. (2013). A quantitative signaling screen identifies CARD11 mutations in the CARD and LATCH domains that induce Bcl10 ubiquitination and human lymphoma cell survival. *Mol. Cell. Biol.* 33, 429–443.
- Coornaert, B., Baens, M., Heynincx, K., Bekaert, T., Haegman, M., Staal, J., Sun, L., Chen, Z.J., Marynen, P., and Beyaert, R. (2008). T cell antigen receptor stimulation induces MALT1 paracaspase-mediated cleavage of the NF- κ B inhibitor A20. *Nat. Immunol.* 9, 263–271.
- Cruciat, C.M. (2014). Casein kinase 1 and Wnt/ β -catenin signaling. *Curr. Opin. Cell Biol.* 31, 46–55.
- Dai, B., Grau, M., Juillard, M., Klener, P., Höring, E., Molinsky, J., Schimmack, G., Aukema, S.M., Hoster, E., Vogt, N., et al. (2017). B-cell receptor-driven MALT1 activity regulates MYC signaling in mantle cell lymphoma. *Blood* 129, 333–346.
- Düwel, M., Welteke, V., Oeckinghaus, A., Baens, M., Kloo, B., Ferch, U., Darney, B.G., Ruland, J., Marynen, P., and Krappmann, D. (2009). A20 negatively regulates T cell receptor signaling to NF- κ B by cleaving Malt1 ubiquitin chains. *J. Immunol.* 182, 7718–7728.
- Eitelhuber, A.C., Warth, S., Schimmack, G., Düwel, M., Hadian, K., Demski, K., Beisker, W., Shinohara, H., Kurosaki, T., Heissmeyer, V., and Krappmann, D. (2011). Dephosphorylation of Carma1 by PP2A negatively regulates T-cell activation. *Embo. J.* 30, 594–605.
- Eitelhuber, A.C., Vasyka, O., Nagel, D., Bognar, M., Lenze, D., Lammens, K., Schlauderer, F., Hlahla, D., Hopfner, K.P., Lenz, G., et al. (2015). Activity-based probes for detection of active MALT1 paracaspase in immune cells and lymphomas. *Chem. Biol.* 22, 129–138.
- Ferch, U., Kloo, B., Gewies, A., Pfänder, V., Düwel, M., Peschel, C., Krappmann, D., and Ruland, J. (2009). Inhibition of MALT1 protease activity is selectively toxic for activated B cell-like diffuse large B cell lymphoma cells. *J. Exp. Med.* 206, 2313–2320.
- Gehring, T., Seeholzer, T., and Krappmann, D. (2018). BCL10—bridging cards to immune activation. *Front. Immunol.* 9, 1539.
- Gewies, A., Gorka, O., Bergmann, H., Pechloff, K., Petermann, F., Jeltsch, K.M., Rudelius, M., Kriegsmann, M., Weichert, W., Horsch, M., et al. (2014). Uncoupling Malt1 threshold function from paracaspase activity results in destructive autoimmune inflammation. *Cell Rep.* 9, 1292–1305.
- Grosche, A., Hauser, A., Lepper, M.F., Mayo, R., von Toerne, C., Merl-Pham, J., and Hauck, S.M. (2016). The Proteome of Native Adult Müller Glial Cells From Murine Retina. *Mol. Cell. Proteomics* 15, 462–480.
- Hailfinger, S., Lenz, G., Ngo, V., Posvitz-Fejfar, A., Rebeaud, F., Guzzardi, M., Penas, E.M., Dierlamm, J., Chan, W.C., Staudt, L.M., and Thome, M. (2009). Essential role of MALT1 protease activity in activated B cell-like diffuse large B-cell lymphoma. *Proc. Natl. Acad. Sci. USA* 106, 19946–19951.
- Hailfinger, S., Nogai, H., Pelzer, C., Jaworski, M., Cabalzar, K., Charton, J.E., Guzzardi, M., Décaillet, C., Grau, M., Dörken, B., et al. (2011). Malt1-dependent RelB cleavage promotes canonical NF- κ B activation in lymphocytes and lymphoma cell lines. *Proc. Natl. Acad. Sci. USA* 108, 14596–14601.
- Jaworski, M., and Thome, M. (2016). The paracaspase MALT1: biological function and potential for therapeutic inhibition. *Cell. Mol. Life Sci.* 73, 459–473.
- Jaworski, M., Marsland, B.J., Gehrig, J., Held, W., Favre, S., Luther, S.A., Perroud, M., Golshayan, D., Gaide, O., and Thome, M. (2014). Malt1 protease inactivation efficiently dampens immune responses but causes spontaneous autoimmunity. *EMBO J.* 33, 2765–2781.
- Jeltsch, K.M., Hu, D., Brenner, S., Zöller, J., Heinz, G.A., Nagel, D., Vogel, K.U., Rehage, N., Warth, S.C., Edelmann, S.L., et al. (2014). Cleavage of roquin and regnase-1 by the paracaspase MALT1 releases their cooperatively repressed targets to promote T(H)17 differentiation. *Nat. Immunol.* 15, 1079–1089.
- Klein, T., Fung, S.Y., Renner, F., Blank, M.A., Dufour, A., Kang, S., Bolger-Munro, M., Scurl, J.M., Priatel, J.J., Schweigler, P., et al. (2015). The paracaspase MALT1 cleaves HOIL1 reducing linear ubiquitination by LUBAC to dampen lymphocyte NF- κ B signalling. *Nat. Commun.* 6, 8777.
- Knies, N., Alankus, B., Weilemann, A., Tzankov, A., Brunner, K., Ruff, T., Kremer, M., Keller, U.B., Lenz, G., and Ruland, J. (2015). Lymphomagenic CARD11/BCL10/MALT1 signaling drives malignant B-cell proliferation via cooperative NF- κ B and JNK activation. *Proc. Natl. Acad. Sci. USA* 112, E7230–E7238.
- Lenz, G., Davis, R.E., Ngo, V.N., Lam, L., George, T.C., Wright, G.W., Dave, S.S., Zhao, H., Xu, W., Rosenwald, A., et al. (2008). Oncogenic CARD11 mutations in human diffuse large B cell lymphoma. *Science* 319, 1676–1679.
- Meininger, I., and Krappmann, D. (2016). Lymphocyte signaling and activation by the CARMA1-BCL10-MALT1 signalosome. *Biol. Chem.* 397, 1315–1333.
- Meininger, I., Griesbach, R.A., Hu, D., Gehring, T., Seeholzer, T., Bertossi, A., Kranich, J., Oeckinghaus, A., Eitelhuber, A.C., Greczmiel, U., et al. (2016). Alternative splicing of MALT1 controls signalling and activation of CD4(+) T cells. *Nat. Commun.* 7, 11292.
- Nagel, D., Spranger, S., Vincendeau, M., Grau, M., Raffegerst, S., Kloo, B., Hlahla, D., Neuschwander, M., Peter von Kries, J., Hadian, K., et al. (2012). Pharmacologic inhibition of MALT1 protease by phenothiazines as a therapeutic approach for the treatment of aggressive ABC-DLBCL. *Cancer Cell* 22, 825–837.
- Nagel, D., Bognar, M., Eitelhuber, A.C., Kutzner, K., Vincendeau, M., and Krappmann, D. (2015). Combinatorial BTK and MALT1 inhibition augments killing of CD79 mutant diffuse large B cell lymphoma. *Oncotarget* 6, 42232–42242.
- Ngo, V.N., Davis, R.E., Lamy, L., Yu, X., Zhao, H., Lenz, G., Lam, L.T., Dave, S., Yang, L., Powell, J., and Staudt, L.M. (2006). A loss-of-function RNA interference screen for molecular targets in cancer. *Nature* 441, 106–110.
- Oeckinghaus, A., Wegener, E., Welteke, V., Ferch, U., Arslan, S.C., Ruland, J., Scheiderei, C., and Krappmann, D. (2007). Malt1 ubiquitination triggers NF- κ B signaling upon T-cell activation. *EMBO J.* 26, 4634–4645.
- Pelzer, C., Cabalzar, K., Wolf, A., Gonzalez, M., Lenz, G., and Thome, M. (2013). The protease activity of the paracaspase MALT1 is controlled by mono-ubiquitination. *Nat. Immunol.* 14, 337–345.
- Phelan, J.D., Young, R.M., Webster, D.E., Roulland, S., Wright, G.W., Kasbekar, M., Shaffer, A.L., 3rd, Ceribelli, M., Wang, J.Q., Schmitz, R., et al. (2018). A multiprotein supercomplex controlling oncogenic signalling in lymphoma. *Nature* 560, 387–391.
- Qiao, Q., Yang, C., Zheng, C., Fontán, L., David, L., Yu, X., Bracken, C., Rosen, M., Melnick, A., Egelman, E.H., and Wu, H. (2013). Structural architecture of the CARMA1/Bcl10/MALT1 signalosome: nucleation-induced filamentous assembly. *Mol. Cell* 51, 766–779.

- Rebeaud, F., Haifinger, S., Posevitz-Fejfar, A., Tapernoux, M., Moser, R., Rueda, D., Gaide, O., Guzzardi, M., Iancu, E.M., Rufer, N., et al. (2008). The proteolytic activity of the paracaspase MALT1 is key in T cell activation. *Nat. Immunol.* *9*, 272–281.
- Satpathy, S., Wagner, S.A., Bell, P., Gupta, R., Kristiansen, T.A., Malinova, D., Francavilla, C., Tolar, P., Bishop, G.A., Hostager, B.S., and Choudhary, C. (2015). Systems-wide analysis of BCR signalosomes and downstream phosphorylation and ubiquitylation. *Mol. Syst. Biol.* *11*, 810.
- Scharschmidt, E., Wegener, E., Heissmeyer, V., Rao, A., and Krappmann, D. (2004). Degradation of Bcl10 induced by T-cell activation negatively regulates NF-kappa B signaling. *Mol. Cell. Biol.* *24*, 3860–3873.
- Schlauderer, F., Seeholzer, T., Desfosses, A., Gehring, T., Strauss, M., Hopfner, K.-P., Gutsche, I., Krappmann, D., and Lammens, K. (2018). Molecular architecture and regulation of BCL10-MALT1 filaments. *Nat. Commun.* *9*, 4041.
- Schmidt-Ullrich, R., Mémet, S., Lilienbaum, A., Feuillard, J., Raphaël, M., and Israel, A. (1996). NF-kappaB activity in transgenic mice: developmental regulation and tissue specificity. *Development* *122*, 2117–2128.
- Seeholzer, T., Kurz, S., Schlauderer, F., Woods, S., Gehring, T., Widmann, S., Lammens, K., and Krappmann, D. (2018). BCL10-CARD11 fusion mimics an active CARD11 seed that triggers constitutive BCL10 oligomerization and lymphocyte activation. *Front. Immunol.* *9*, 2695.
- Shinohara, H., Maeda, S., Watarai, H., and Kurosaki, T. (2007). IkappaB kinase beta-induced phosphorylation of CARMA1 contributes to CARMA1 Bcl10 MALT1 complex formation in B cells. *J. Exp. Med.* *204*, 3285–3293.
- Shinohara, H., Behar, M., Inoue, K., Hiroshima, M., Yasuda, T., Nagashima, T., Kimura, S., Sanjo, H., Maeda, S., Yumoto, N., et al. (2014). Positive feedback within a kinase signaling complex functions as a switch mechanism for NF- κ B activation. *Science* *344*, 760–764.
- Sommer, K., Guo, B., Pomerantz, J.L., Bandaranayake, A.D., Moreno-García, M.E., Ovechkina, Y.L., and Rawlings, D.J. (2005). Phosphorylation of the CARMA1 linker controls NF-kappaB activation. *Immunity* *23*, 561–574.
- Staal, J., Driège, Y., Bekaert, T., Demeyer, A., Muyliaert, D., Van Damme, P., Gevaert, K., and Beyaert, R. (2011). T-cell receptor-induced JNK activation requires proteolytic inactivation of CYLD by MALT1. *EMBO J.* *30*, 1742–1752.
- Sun, L., Deng, L., Ea, C.K., Xia, Z.P., and Chen, Z.J. (2004). The TRAF6 ubiquitin ligase and TAK1 kinase mediate IKK activation by BCL10 and MALT1 in T lymphocytes. *Mol. Cell* *14*, 289–301.
- Traenckner, E.B., Pahl, H.L., Henkel, T., Schmidt, K.N., Wilk, S., and Baeuerle, P.A. (1995). Phosphorylation of human I kappa B-alpha on serines 32 and 36 controls I kappa B-alpha proteolysis and NF-kappa B activation in response to diverse stimuli. *EMBO J.* *14*, 2876–2883.
- Uehata, T., Iwasaki, H., Vandebon, A., Matsushita, K., Hernandez-Cuellar, E., Kuniyoshi, K., Satoh, T., Mino, T., Suzuki, Y., Standley, D.M., et al. (2013). Malt1-induced cleavage of regnase-1 in CD4(+) helper T cells regulates immune activation. *Cell* *153*, 1036–1049.
- Venerando, A., Ruzzene, M., and Pinna, L.A. (2014). Casein kinase: the triple meaning of a misnomer. *Biochem. J.* *460*, 141–156.
- Wang, D., You, Y., Case, S.M., McAllister-Lucas, L.M., Wang, L., DiStefano, P.S., Nuñez, G., Bertin, J., and Lin, X. (2002). A requirement for CARMA1 in TCR-induced NF-kappa B activation. *Nat. Immunol.* *3*, 830–835.
- Wegener, E., Oeckinghaus, A., Papadopoulou, N., Lavitas, L., Schmidt-Suppran, M., Ferch, U., Mak, T.W., Ruland, J., Heissmeyer, V., and Krappmann, D. (2006). Essential role for IkappaB kinase beta in remodeling Carma1-Bcl10-Malt1 complexes upon T cell activation. *Mol. Cell* *23*, 13–23.
- Wiesmann, C., Leder, L., Blank, J., Bernardi, A., Melkko, S., Decock, A., D’Arcy, A., Villard, F., Erbel, P., Hughes, N., et al. (2012). Structural determinants of MALT1 protease activity. *J. Mol. Biol.* *419*, 4–21.
- Wiśniewski, J.R., Zougman, A., Nagaraj, N., and Mann, M. (2009). Universal sample preparation method for proteome analysis. *Nat. Methods* *6*, 359–362.

STAR★METHODS

KEY RESOURCES TABLE

REAGENT or RESOURCE	SOURCE	IDENTIFIER
Antibodies		
Goat polyclonal anti-Actin (I-19) HRP	Santa Cruz Biotechnology	Cat#sc1616 HRP; RRID: N/A
Rabbit monoclonal anti-BCL10 (EP606Y)	Abcam	Cat#ab33905; RRID: AB_725640
Goat polyclonal anti-BCL10 (C-17)	Santa Cruz Biotechnology	Cat#sc9560; RRID: AB_2064858
Rabbit monoclonal anti-CARD11 (1D12)	Cell Signaling Technology	Cat#4435; RRID: AB_10694496
Goat polyclonal anti-CK1 alpha (C-19)	Santa Cruz Biotechnology	Cat#sc6477; RRID: AB_637734
Rabbit monoclonal anti-CK1 alpha (EPR1961)	Abcam	Cat#ab108296; RRID: AB_10864123
Rabbit monoclonal anti-CK1 alpha (EPR19824)	Abcam	Cat#ab206652; RRID: N/A
Mouse monoclonal anti-CK1 alpha (H-7)	Santa Cruz Biotechnology	Cat#sc74582; RRID: AB_2084662
Mouse monoclonal anti-CYLD (E10)	Santa Cruz Biotechnology	Cat#sc74435; RRID: AB_1122022
Rabbit polyclonal anti-ERK (442704)	Merck Millipore	Cat#M5670; RRID: AB_477216
Sheep polyclonal anti-HOIL-1/RBCK1	MRC PPU Reagents and Services	Cat#S105D; RRID: N/A
Mouse monoclonal anti-I κ B α (L35A5)	Cell Signaling Technology	Cat#4814; RRID: AB_390781
Rabbit polyclonal anti-IKK γ (FL-419)	Santa Cruz Biotechnology	Cat#sc-8330; RRID: AB_2124846
Rabbit polyclonal anti-JNK1/2	Cell Signaling Technology	Cat#9252; RRID: AB_2250373
Mouse monoclonal anti-MALT1 (B12)	Santa Cruz Biotechnology	Cat#sc-46677; RRID: AB_627909
Rabbit polyclonal anti-MALT1 (H300)	Santa Cruz Biotechnology	Cat#sc-28246; RRID: AB_2139156
Rat anti-MALT1 (21A2)	Core facility monoclonal antibodies HMGU	RRID: N/A
Rat anti-MALT1 (17C11)	Core facility monoclonal antibodies HMGU	RRID: N/A
Rat anti-MALT1B S562 (29E9)	Core facility monoclonal antibodies HMGU	RRID: N/A
Mouse anti-MALT1 S649 (29E12)	Core facility monoclonal antibodies HMGU	RRID: N/A
Rat anti-MALT1 S803 (24A4)	Core facility monoclonal antibodies HMGU	RRID: N/A
Rabbit polyclonal anti-p38 (C-20)	Santa Cruz Biotechnology	Cat#sc-535; RRID: AB_632138
Rabbit anti-phospho-CARD11 S645	Shinohara et al., 2007	RRID: N/A
Rabbit polyclonal anti-phospho-ERK	Cell Signaling Technology	Cat#9101; RRID: AB_331646
Mouse monoclonal anti-phospho-I κ B α (Ser32/36) (5A5)	Cell Signaling Technology	Cat#9246; RRID: AB_2151442
Rabbit monoclonal anti-phospho-JNK (81E11)	Cell Signaling Technology	Cat#4668; RRID: AB_823588
Rabbit polyclonal anti-phospho-p38	Cell Signaling Technology	Cat#9211; RRID: AB_331641
Mouse anti-Regnase1/MCPIP1 (604421)	R&D System	Cat#MAB7875; RRID: N/A
Mouse monoclonal anti-ubiquitin (P4D1)	Santa Cruz Biotechnology	Cat#sc-8017; RRID: AB_2315523
Rat anti-HA (3F1)	Core facility monoclonal antibodies HMGU	RRID: N/A
Hamster anti-mouse anti-CD3 (145-2C11)	BD Bioscience	Cat#557306; RRID: AB_396632
Hamster anti-mouse anti-CD28 (37.51)	BD Bioscience	Cat#553295; RRID: AB_394764
Rabbit anti-hamster IgG (H+L)	Jackson ImmunoResearch	Cat#307-005-003; RRID: AB_2339572
Rat anti-mouse anti-CD16/32	eBioscience	Cat#14-0161-81; RRID: AB_467132
Rat monoclonal anti-mouse IL-2 (JES6-5H4)	eBioscience	Cat#11-7021-82; RRID: AB_465382
Rat monoclonal anti-mouse IgG1-FITC (A85-1)	eBioscience	Cat#553443; RRID: AB_394862
Mouse anti-Thy1.1-APC (HIS51)	eBioscience	Cat#17-0900-82; RRID: AB_469420
Mouse anti-human anti-CD3	BD Pharmigen	Cat#555336; RRID: AB_395742
Mouse anti-human anti-CD28	BD Pharmigen	Cat#555725; RRID: AB_396068
Rat anti-mouse IgG1	BD Pharmigen	Cat#553440; RRID: AB_394860
Rat anti-mouse IgG2a	BD Pharmigen	Cat#553387; RRID: AB_394825
HRP-conjugated anti-rabbit	Jackson ImmunoResearch	Cat#711-035-152; RRID: AB_10015282

(Continued on next page)

Continued

REAGENT or RESOURCE	SOURCE	IDENTIFIER
HRP-conjugated anti-mouse	Jackson ImmunoResearch	Cat#715-035-150; RRID: AB_2340770
HRP-conjugated anti-goat	Jackson ImmunoResearch	Cat#805-035-180; RRID: AB_2340874
HRP-conjugated anti-rat	Jackson ImmunoResearch	Cat#112-035-062; RRID: AB_2338133
HRP-conjugated anti-sheep	Jackson ImmunoResearch	Cat#313-035-003; RRID: AB_2339948
Bacterial and Virus Strains		
<i>E. coli</i> BL21-CodonPlus (DE3)-RIPL	Agilent Technologies	Cat#230280
One Shot TOP10 Chemically Competent <i>E. coli</i>	Thermo Fisher Scientific	Cat#C404003
One Shot Stbl3 Chemically Competent <i>E. coli</i>	Thermo Fisher Scientific	Cat#C737303
Chemicals, Peptides, and Recombinant Proteins		
Recombinant human TNF alpha	biomol	Cat#50435.50
Recombinant human GST-CK1 alpha	Sigma-Aldrich	Cat#SRP5013
Recombinant human GST-MALT1 (aa 325-760)	Laboratory of Daniel Krappmann	N/A
Recombinant human 6xHis-MALT1A 334-824-GyrB-HA	Laboratory of Z.J. Chen, University of Texas	N/A
Cys-EYSAEpSLVRNL (MALT1B S562)	Peps4LifeScience	Custom made
Cys-GSYLVpSKDLPK (MALT1B S649)	Peps4LifeScience	Custom made
Cys-DEIPFPpSFSDRL (MALT1 S803)	Peps4LifeScience	Custom made
cOmplete, Mini, EDTA-free Protease Inhibitor Cocktail	Roche	Cat#11836170001
Pierce High Capacity Streptavidin Agarose	Thermo Fisher Scientific	Cat#20357
Strep-Tactin Sepharose 50% suspension	IBA	Cat#2-1201-010
rec-Protein G Sepharose 4B beads	Life technologies	Cat#101241
Red blood cell (RBC) lysis buffer	Miltenyi Biotec	Cat#130-094-183
X-tremeGENE HP DNA Transfection Reagent	Roche Diagnostics	Cat#6366236001
Polybrene	Sigma-Aldrich	Cat#TR-1003-G
Phorbol 12-myristate 13-acetate (PMA)	Merck Millipore	Cat#524400-1; CAS 16561-29-8
Ionomycin	Calbiochem	Cat#407950-1; CAS 56092-82-1
Brefeldin-A	Sigma-Aldrich	Cat#B6542; CAS 20350-15-6
Paraformaldehyde	Roth	Cat#0335.1; CAS 30525-89-4
Saponin	Roth	Cat#4185.1; CAS 232-462-6
Roti-Load 1, 4x conc.	Carl Roth	Cat#K929.1
Dimethylsulfoxide	Biosolve	Cat#04470501, CAS 67-68-5
Proleukin®S (Aldesleukin; recombinant IL-2)	Novartis Pharma	PZN #02238131
Critical Commercial Assays		
Murine CD4+ T cell isolation kit	Miltenyi Biotec	Cat#130-104-454
Human CD4+ T cell isolation kit	Miltenyi Biotec	Cat#130-096-533
Dual-luciferase reporter assay	Promega	Cat#E1910
CD90.1 MicroBead	Miltenyi Biotec	Cat#130-121-273
RNeasy Mini Kit	QIAGEN	Cat#74106
Verso cDNA Synthesis Kit	Thermo Fisher Scientific	Cat#AB1453A
2x Takyon qPCR Kit SYBR Assay	Eurogentec	Cat#UF-NSMT-B0701
Experimental Models: Cell Lines		
HEK293 cells	DSMZ	RRID: CVCL_0045
HEK293T cells	DSMZ	RRID: CVCL_0063
Jurkat T cells	Laboratory of Lienhard Schmitz (University of Giessen)	Verified by DSMZ
MALT1-deficient Jurkat T cells	Laboratory of Daniel Krappmann	Meininger et al., 2016
CARD11-deficient Jurkat T cells	Laboratory of Daniel Krappmann	Seeholzer et al., 2018

(Continued on next page)

Continued

REAGENT or RESOURCE	SOURCE	IDENTIFIER
CK1 alpha-deficient Jurkat T cells	This paper	N/A
BCL10-deficient Jurkat T cells	Laboratory of Daniel Krappmann	Schlauderer et al., 2018
JPM50.6	Laboratory of Xin Lin (Tsinghua University)	N/A
HBL1	Laboratory of Georg Lenz (University of Münster)	Nagel et al., 2012
TMD8	Laboratory of Georg Lenz (University of Münster)	Nagel et al., 2012
OCI-Ly3	DSMZ	ACC 761, Lot 4
OCI-Ly10	Laboratory of Georg Lenz University of Münster)	Nagel et al., 2012
U2932	DSMZ	ACC 633, Lot 9
BJAB	DSMZ	ACC 757, Lot 4
SUDHL4	DSMZ	ACC 495, Lot 11
SUDHL6	DSMZ	ACC 572, Lot 7
HBL1 CARD11 WT	Laboratory of Daniel Krappmann	Nagel et al., 2015
HBL1 CARD11 L225LI	Laboratory of Daniel Krappmann	Nagel et al., 2015
Phoenix cells	Laboratory of Vigo Heissmeyer (Ludwig Maximilians-University, Munich)	N/A
Experimental Models: Organisms/Strains		
MALT1 ^{tm1a(EUCOMM)Hmg} (C57BL/6N-A/a)	EUCOMM	ES cell clone: HEPD0618_3_D10
Oligonucleotides		
CK1 alpha exon 3 sgRNA #1	Metabion	N/A
NF-kB (H2K) fw (EMSA probe)	Eurofins	N/A
NF-kB (H2K) rev (EMSA probe)	Eurofins	N/A
OCT1 fw (EMSA probe)	Eurofins	N/A
OCT1 rev (EMSA probe)	Eurofins	N/A
qPCR Primer (IL-2, A20, IκBα, β-Actin)	Eurofins	N/A
Recombinant DNA		
pEF 3xFLAG mock	Laboratory of Daniel Krappmann	Scharschmidt et al., 2004
pEF 3xFL-MALT1	Laboratory of Daniel Krappmann	Oeckinghaus et al., 2007
pEF 3xFL-BCL10	Laboratory of Daniel Krappmann	Wegener et al., 2006
pEF 3xFL-CK1α	This paper	N/A
pEF CARD11-FS	Laboratory of Daniel Krappmann	Bognar et al., 2016
pEF HA-MALT1	Laboratory of Daniel Krappmann	Oeckinghaus et al., 2007
pEF HA-CARD11	Laboratory of Daniel Krappmann	Eitelhuber et al., 2011
pX458_CK1α exon 3 sgRNA #1	This paper; pX458 was a gift from Feng Zhang	Addgene #48138
pHAGE_hΔCD2-T2A-CK1α WT-FS	This paper	N/A
pHAGE_hΔCD2-T2A-CK1α D136N-FS	This paper	N/A
pHAGE_hΔCD2-T2A-CK1α Y292A-FS	This paper	N/A
pHAGE_hΔCD2-T2A-MALT1B WT-FS	This paper	N/A
pHAGE_hΔCD2-T2A-MALT1B S559/562A-FS	This paper	N/A
pHAGE_hΔCD2-T2A-MALT1B S645/649A-FS	This paper	N/A
pHAGE_hΔCD2-T2A-MALT1B S803/805A-FS	This paper	N/A
pHAGE_hΔCD2-T2A-MALT1B 6x S/A-FS	This paper	N/A
pHAGE_hΔCD2-T2A-MALT1B S559/562D-FS	This paper	N/A
pHAGE_hΔCD2-T2A-MALT1B S645/649D-FS	This paper	N/A
pHAGE_hΔCD2-T2A-MALT1B S803/805D-FS	This paper	N/A

(Continued on next page)

Continued

REAGENT or RESOURCE	SOURCE	IDENTIFIER
pHAGE_hΔCD2-T2A-MALT1B 6x S/D-FS	This paper	N/A
pMD2.G	Laboratory of Didier Trono	Addgene #12259
psPAX2	Laboratory of Didier Trono	Addgene #12260
pMSCV_MALT1B WT-FS_IRES_Thy1.1	This paper	N/A
pMSCV_MALT1B S559/562A-FS_IRES_Thy1.1	This paper	N/A
pMSCV_MALT1B S645/649A-FS_IRES_Thy1.1	This paper	N/A
pMSCV_MALT1B S803/805A-FS_IRES_Thy1.1	This paper	N/A
pMSCV_MALT1B 6x S/A-FS_IRES_Thy1.1	This paper	N/A
Software and Algorithms		
Prism5 and 7	GraphPad	https://www.graphpad.com/scientific-software/prism/
FlowJo V10	FlowJo LLC	https://www.flowjo.com/solutions/flowjo/
ScanSite 4.0	Laboratory of Micheal B. Yaffe (Koch Institute, MIT)	https://scansite4.mit.edu/4.0/#home
Proteome Discoverer Software	Thermo Fisher Scientific	Version 1.4.1.14
Mascot	Matrix Science	Version 2.5.1
PhosphoRS		Version 3.0
LabImage 1D	Kapelan Bio-Imaging	Version 1.5
Other		
DMEM (high glucose, L-glutamine)	Life Technologies	Cat#11965092
RPMI 1640 Medium (L-glutamine)	Life Technologies	Cat#21875034
0.05% trypsin/EDTA solution	Life Technologies	Cat#25300054
FBS	Life Technologies	Cat#10500056
Penicillin/Streptomycin (10000 U/ml)	Life Technologies	Cat#15140148
Non-essential amino acids solution (NEAA) 100x	Life Technologies	Cat#11140050
L-glutamine (200 mM)	Life Technologies	Cat#25030081
Sodium pyruvate (100 mM)	Life Technologies	Cat#11360070
S-Monovette 9ml LH	Sarstadt	Cat#02.1065.001
Lymphoprep	StemCell Technologies, Inc.	Cat#07801

LEAD CONTACT AND MATERIALS AVAILABILITY

Further information and requests for resources and reagents should be directed to and will be fulfilled by the Lead Contact, Daniel Krappmann (daniel.krappmann@helmholtz-muenchen.de). All reagents developed for this study are available under Material Transfer Agreements from Helmholtz Zentrum München.

EXPERIMENTAL MODELS AND SUBJECT DETAILS

Cell culture

Adherent HEK293, HEK293T and Phoenix cells were cultured in DMEM supplemented with 10% FCS and 100 U/ml P/S. Cells were passaged after they reached 80% confluency. To detach cells from dishes, cells were washed with PBS and treated with 1-3 mL 0.05% trypsin/EDTA solution for approximately 5 min. The reaction was halted by the addition of fresh DMEM. Cells were then diluted in flasks or seeded in appropriate dishes for further experiments. For cultivation of the suspension Jurkat T cells and CARMA1-deficient JPM50.6 T cells, RPMI medium supplemented with 10% FCS and 100 U/ml P/S was used. Jurkat T cells were maintained at a density between 0.5x and 1.5x 10⁶ cells/ml. Prior to each experiment, the cells were maintained at a density of approximately 1x 10⁶ cells/ml. DLBCL cell lines were cultivated in RPMI medium supplemented with 15% FCS and 100 U/ml P/S. Cells were maintained at a density between 0.5x and 1.5x 10⁶ cells/ml. Primary murine and human CD4 T cells were cultured in RPMI medium supplemented with 10% heat-inactivated FCS, 1% P/S, 1% NEAA, 1% HEPES (pH 7.4), 1% L-glutamine, 1% sodium pyruvate and 0.1% β-mercapto-ethanol.

Isolation and cultivation of primary murine CD4 T cells

For stimulation and knockdown experiments, primary murine CD4 T cells were isolated from spleen and lymph nodes (axial, inguinal and neck) of MALT1 KO mice (MALT1^{tm1a(EUCOMM)Hmgu}, ES cell clone HEPD0671_C08) by negative magnetic-activated cell sorting (MACS) selection using the murine CD4 T cell isolation kit (Miltenyi Biotec). First, spleen and lymph nodes were placed in primary T cell medium and ground through a cell strainer (100 μ M). To separate the cells from residual tissue particles, the homogenate was pelleted by centrifugation (300x g, 5 min). Afterward, the pellet was re-suspended in 500 μ l DMEM and incubated with 5 mL RBC lysis buffer (Miltenyi Biotec) for 2 min at RT, in order to destroy erythrocytes. Samples were washed, centrifuged and re-filtered through a cell strainer to further eliminate residual tissue particles. CD4 T cells were then purified according to the manufacturer's protocol. The separated CD4 T cells were pelleted and re-suspended in an appropriate volume of primary T cell medium (cell density 0.5x 10⁶ cells/ml). For expansion of primary murine CD4 T cells, the medium was supplemented with 1:5000 recombinant IL-2 (Pro-leukin®S, Novartis Pharma).

Isolation and cultivation of primary human CD4 T cells

For isolation of human CD4 T cells, blood was taken from healthy donors into S-Monovette (Sarstedt) columns containing Lithium-Heparin. Blood was centrifuged (300x g, 10 min, RT, no break) to separate the plasma (upper layer), buffy coat (intermediate layer), and erythrocytes (lowest layer). Following removal of the plasma fraction, the intermediate buffy coat layer containing leukocytes and platelets was collected (approx. 10-18 ml/50 mL blood) and diluted with PBS up to a volume of 35 ml. To isolate mononuclear cells (MNCs), diluted buffy coat was carefully layered onto 15 mL Lymphoprep density gradient medium (StemCell Technologies, Inc.) and centrifuged (160x g, 20 min, RT, no break). About 20 mL of supernatant was carefully removed and the sample was again centrifuged (350x g, 20 min, RT, no break). Finally, the intermediate layer containing the MNCs was collected and washed twice with PBMC buffer B1 (300x g, 8 min, 4°C). CD4⁺ T cells were isolated by negative MACS selection using the human CD4 T cell isolation kit (Miltenyi Biotec) according to the manufacturer's instructions. Purified cells were re-suspended in primary T cell medium at a density of 2x 10⁶ cells/ml and used for further stimulation experiments. Written consent and approval by the ethics board of the Medical Faculty at the Technical University Munich was obtained for the use of peripheral blood from healthy donors.

METHOD DETAILS

Generation of CK1 α -deficient Jurkat T cells

Jurkat T cells were transfected by electroporation with plasmid pX458 (Addgene #48138, gift F. Zhang) bearing Cas9 and designed sgRNA (5'- TGTACTTATGTTAGCTGACC) using a Gene Pulser Xcell (BioRad) (220 V, 1000 μ F, 0.4 cm cuvettes). After 24 h of incubation, EGFP-positive cells were sorted using a MoFlo sorting system (Beckman Coulter). Using serial dilution, selected cells were plated in 96 well plates with a density of 0.5, 2 or 5 cells/well, and incubated for one to two weeks at 37°C and 5% CO₂. Growing cell clones were then selected and further expanded. KO cell clones were initially identified by anti-CK1 α staining by Western Blot. Clones lacking protein expression were genotyped by genomic PCR and sequencing.

Lentiviral transduction of Jurkat T cells

To generate stable MALT1-expressing cell lines, MALT1-deficient Jurkat T cells were lentivirally transduced with different pHAGE-h Δ CD2-T2A-MALT1 constructs. First, lentivirus was produced by co-transfecting HEK293T cells with MALT1 expression plasmids and lentiviral packaging vectors: 1.5x 10⁶ HEK293T cells were seeded in a 10 cm² dish in 8 mL DMEM medium one day prior to transfection. The following day, HEK293T cells were transfected with 1 μ g of the lentiviral envelope plasmid pMD2.G (Addgene #12259; gift D. Trono), 1.5 μ g of the packaging vector psPAX2 (Addgene #12260; gift D. Trono), and 2 μ g MALT1 transfer plasmid (pHAGE-h Δ CD2-T2A-MALT1-StrepTagII) using X-tremeGENE HP DNA Transfection Reagent (Roche Diagnostics) according to the manufacturer's instructions. After 3 days, the supernatant containing the virus particles was removed and sterile filtered (0.45 μ M). 500 μ l, 1000 μ l or 1500 μ l virus together with 8 μ g/ml polybrene was added to 2x 10⁵ MALT1-deficient Jurkat T cells. 24 h later, cells were washed with PBS (three times) and re-suspended in 1 mL fresh RPMI medium. After one week in culture, transduction efficiency was assessed by analyzing h Δ CD2 expression using flow cytometry, and by checking MALT1 expression levels via Western Blot. When comparing several mutants similar expression levels were used.

Retroviral reconstitution of CD4 T cells from MALT1 KO mice

Retroviruses were produced in Phoenix cells transfected with pMSCV retroviral transfer vectors carrying human MALT1-FlagStrepII constructs and Thy1.1 (separated by internal ribosome entry site (IRES) sequence). Virus supernatants were collected after 48 and 72 h and combined. Prior to the infection, CD4 T cells were stimulated for 48 h using hamster anti-murine anti-CD3 (0.5 μ g/ml) and hamster anti-murine anti-CD28 (1 μ g/ml) on anti-hamster pre-coated plates. For infection, CD4 T cells were incubated for 6 h with retroviral supernatant supplemented with Polybrene (8 μ g/ml) and then washed using RPMI medium. Cultivation and expansion of primary murine CD4 T cells was performed as described above.

Retroviral transduction of MALT1 shRNA and rescue in DLBCL

For retroviral transductions, DLBCL cell lines were transduced with a feline endogenous virus (FEV) to express a murine ecotropic receptor using bleomycin as a selectable marker. To allow doxycycline-inducible small hairpin RNA (shRNA) expression, ecotropic receptor-expressing cell lines were secondarily infected with a retrovirus expressing the bacterial tetracycline repressor (TETR) using hygromycin as selection marker (Ngo et al., 2006). For the MALT1 rescue experiment, these cells were stably transduced with a retroviral MALT1 shRNA (targeting sequence GTCACAGAATTGAGTGATTTTC) cloned in pRSMX vector (Dai et al., 2017). Expression of the shRNA was induced by adding 20 ng/ml doxycycline. Cells carrying the MALT1 shRNA were subsequently transduced to constitutively express Strep-tagged MALT1 WT, MALT1 S559/562A, MALT1 S645/649A, MALT1 S803/805A or MALT1 6xSA together with a GFP reporter protein using a pMSCV-IRES-GFP plasmid. To ensure that only endogenous MALT1 was knocked down, the silent mutations in shRNA binding site of the exogenously expressed variants at cDNA position 313 (GAATTG to GAGTTA) were introduced, without changing the amino acid sequence (Pelzer et al., 2013). The double-transduced cells were monitored for live GFP-positive cells by flow cytometry and normalized to the value at day 2 post retroviral transduction. Successful expression of the different MALT1 variants was determined using Western Blotting.

Transfection in HEK293 cells

For overexpression experiments, HEK293 cells were transfected using standard calcium phosphate transfection protocols. 2.5×10^6 HEK293 cells were seeded in a 10 cm² dish on the day before transfection.

Electroporation of CARD11 KO Jurkat T cells

For overexpression experiments, CARD11 KO Jurkat T cells were electroporated using a Gene Pulser Xcell (BioRad) (220 V, 1000 μ F, 0.4 cm cuvettes). 5 μ g expression vectors for each construct were used and DNA amount was adjusted using empty expression control, if needed. 48 hours after electroporation, cells were lysed and HA-IP was performed.

Stimulation of Jurkat T cells and primary human CD4 T cells

Jurkat T cells and primary human CD4 T cells were stimulated with P/I (Phorbol 12-myristate 13-acetate (PMA)/Ionomycin) using a concentration of 200 ng/ml PMA and 300 ng/ml Ionomycin. P/I stimulation acts downstream of TCR/CD28 as PMA directly stimulates PKC θ and Ionomycin triggers Ca²⁺ release from the endoplasmic reticulum into the cytosol. Stimulation was performed in tubes at 37°C. Anti-CD3/CD28 stimulation was performed in 300 μ l medium using 1 μ g/ml murine anti-human anti-CD3 antibody (IgG1) and 3 μ g/ml murine anti-human anti-CD28 antibody (IgG2a). The antibodies were cross linked using 3 μ g/ml of anti-mouse IgG1 and anti-mouse IgG2a antibodies. Stimulation was performed in tubes at 37°C. TNF α stimulation was performed in 2 mL medium using a concentration of 20 ng/ml. Stimulation was performed in tubes at 37°C.

Stimulation of primary murine CD4 T cells

Primary murine CD4 T cells were stimulated with P/I or anti-CD3 and anti-CD28 antibodies in primary T cell medium. For P/I stimulation, 200 ng/ml PMA and 300 ng/ml Ionomycin were used. Anti-CD3/CD28 stimulation was performed on pre-coated plates. Therefore plates were coated with rabbit anti-hamster IgG (30 μ l in 1 mL PBS per 6-well) over night at 4°C. Afterward, plates were washed twice with PBS before cells were stimulated with anti-CD3 (0.5 μ g/ml) and anti-CD28 (1 μ g/ml), and added to the pre-coated wells. Cells were stimulated at a density between $1 \times - 5 \times 10^6$ cells per ml.

Generation and analyses of NF- κ B-EGFP reporter Jurkat T cells

Lentiviral NF- κ B reporter was generated by introducing six copies of the NF- κ B/Rel-binding site of the immunoglobulin κ light chain enhancer (ATCTGGGGATTCCCCA) and the conalbumin (cona)minimal promoter upstream of a hygromycin-EGFP-fusion gene (pHAGE-Ig κ (6x)cona-HygEGFP), leading to NF- κ B-dependent expression of EGFP (NF- κ B-EGFP reporter) (Schmidt-Ullrich et al., 1996). To generate parental and MALT1 KO Jurkat T cells expressing the NF- κ B-EGFP reporter, cells were lentivirally transduced as described above. Transduction efficiency of > 95% was assessed by analyzing EGFP expression following TNF α stimulation. The generated MALT1 KO/NF- κ B reporter Jurkat T cells were subsequently lentivirally transduced with different pHAGE-h Δ CD2-T2A-MALT1B constructs as described before. Transduction efficiency of the second transduction was assessed by analyzing h Δ CD2 expression using flow cytometry, and by checking MALT1 expression levels via Western Blot. Stimulation of generated NF- κ B reporter Jurkat T cells were performed in 500 μ l medium in 24-well plates at 37°C. Stimulation conditions were used as described before, but adjusted to the respective medium volume. Cells were stimulated for the stated time and EGFP expression was analyzed by FACS and quantified by gating on the number of EGFP positive cells.

Staining of surface molecules

To assess h Δ CD2 surface expression of infected CK1 α - or MALT1-deficient Jurkat T cells, approximately 0.2×10^6 cells were collected and re-suspended in 400 μ l FACS buffer (1x PBS, 2% FCS (w/v), 0.01% NaN₃ (v/v)). Cells were stained with anti-CD2-APC antibody (human, dilution 1:400) for 15 min at 4°C in the dark. Samples were then washed with FACS buffer, taken up in ca. 200 μ l FACS buffer and acquired on Attune Acoustic Focusing Cytometer.

For staining of Thy1.1 expression in primary murine CD4 T cells, cells ($0.2\text{--}1 \times 10^6$) were collected after stimulation and were re-suspended in FACS buffer. To prevent unspecific antibody binding to Fc receptors, samples were first treated with anti-CD16/32 (mouse, dilution 1:50) for 10 min at 4°C . Afterward, staining with anti-Thy1.1-APC (1:200 dilution) was performed for 10–15 min at 4°C in the dark. Samples were washed, resuspended in FACS buffer and acquired on Attune Cytometer.

Intracellular cytokine staining

For intracellular IL-2 staining, primary murine CD4 T cells (1×10^6) were stimulated for 5 h with P/I or anti-CD3/CD28 in the presence of Brefeldin-A (10 ng/ml, Sigma) to prevent exocytosis of signaling molecules. After stimulation, cells were collected, centrifuged ($300 \times g$, 5 min, 4°C) and stained for the surface marker. Afterward, samples were washed and fixed in 1% PFA for 15 min at RT. Then, cells were washed and permeabilized in IC buffer (0.2% saponin in 1x PBS) for 15 min at RT. Unspecific antibody binding was blocked with anti-CD16/32 (mouse, dilution 1:50 in saponin buffer, 10 min, 4°C) prior to incubation of samples with anti-IL-2-FITC or anti-I κ B α antibodies (both mouse, dilution 1:100 in IC buffer) for 30 min on ice. Cells were then washed ($300 \times g$, 5 min, 4°C) and filled up with FACS buffer to wash out unbound antibodies (> 15 min, RT). Anti-I κ B α treated cells had to be stained with a secondary rat anti-mouse-IgG1-FITC antibody (1:300, 20 min at 4°C in the dark). Samples were again washed ($300 \times g$, 5 min, 4°C), re-suspended in FACS buffer and acquired on Attune Cytometer.

Quantitative analyses of NF- κ B target gene induction

Positive retroviral transduced primary CD4 T cells expressing a human MALT1-FlagStrepII constructs and Thy1.1 surface marker were purified using CD90.1 MicroBeads (Miltenyi) according to the manufacturer's guide. Purified cells were cultured and expanded for two more days as described above. 0.5×10^5 cells were stimulated for 1 and 4 hours with anti-CD3 (0.05 $\mu\text{g}/\text{ml}$) and anti-CD28 (1 $\mu\text{g}/\text{ml}$) antibodies, and added to pre-coated wells (5 $\mu\text{g}/\text{ml}$ rabbit anti-hamster IgG per 6-well; overnight at 4°C). Afterward, cells were collected, washed with PBS and the RNA was isolated using the RNeasy Kit (QIAGEN) according to the manufacturer's guide. RNA was transcribed into cDNA using the Verso cDNA synthesis Kit (Thermo Fisher Scientific) according to the manufacturer's guide. For reverse transcriptase (RT)-PCR the Takyon qPCR Kit for SYBR Assays (Eurogentec) was used and the samples were measured using a LightCycler 480 II instrument (Roche). The following primers were used: IL-2: fw – 5' TGAGCAGGATGGAGAATTACAG, rev – 5' GTGTTGTCAGAGCCCTTTAGTT; TNFAIP3/A20: fw – 5' CTACGACACTCGGAACTGGA, rev – 5' CAAACTTCTTAGCATT TGTCTG; NFKBIA/I κ B α : fw – 5' CCTGCAGCAGACTCCACTC, rev – 5' GACACGTGTGGCCATTGTAG; β -Actin: fw – 5' CACACCCGC CACCAGTTCG, rev – 5' CACCATCACACCCTGGTGC.

Preparation of whole cell lysates

For analysis of protein expression levels and activation of downstream signaling pathways including NF- κ B DNA binding, $1\text{--}3 \times 10^6$ cells were harvested ($300 \times g$, 5 min, 4°C), washed with PBS, and subsequently lysed in 60–120 μl high salt buffer (20 mM HEPES (pH 7.9), 350 mM NaCl, 20% Glycerol (v/v), 1 mM MgCl_2 , 0.5 mM EDTA, 0.1 mM EGTA, 1% NP-40, 1 mM DTT, 10 mM NaF, 8 mM β -Glycerophosphate, 300 μM NaVanadate, Protease inhibitor mix). Lysates were incubated on a shaker for 20 min at 4°C before insoluble cellular debris was removed by centrifugation (14000 rpm, 15–30 min, 4°C). For Western Blot analysis, 4x SDS loading buffer (Roti®-Load1, Roth) was added and samples were boiled for 5 min at 95°C . Aliquots for electrophoretic mobility shift assay (EMSA) were taken before the addition of 4x SDS loading buffer and stored at -80°C .

Co-immunoprecipitation (co-IP) and Strep-Tactin pulldown (ST-PD)

For protein interaction studies, $3\text{--}5 \times 10^7$ cells were lysed in 800 μl Co-IP buffer (25 mM HEPES (pH 7.5), 150 mM NaCl, 1 mM Glycerol, 0.2% NP-40 (v/v), 1 mM DTT, 10 mM NaF, 8 mM β -Glycerophosphate, 300 μM NaVanadate) supplemented with protease inhibitors. Lysates were incubated for 20 min at 4°C in an overhead rotator before samples were cleared by centrifugation (14 000 rpm, 15 min, 4°C). 30 μl supernatant was collected as lysate control and was mixed with 4x SDS loading buffer (Roti®-Load1, Roth) and boiled for 5 min at 95°C . The residual supernatant was used for binding studies. Immunoprecipitations (IPs) were carried out by using antibodies against BCL10 (C-17, 0.5 μg), CK1 α (C-19, 1.5 μg or H-7, 2 μg or EPR19824, 7 μl), HA-tag (30 μl hybridoma supernatant of clone 12CA5, produced by Antibody Core Facility, HMGU), MALT1 (H300, 1.5 μg or B-12, 1.5 μg or 250 μl hybridoma supernatant of clone 21A2, produced by Antibody Core Facility, HMGU), MALT1 pS803 (250 μl hybridoma supernatant of clone 24A4, produced by Antibody Core Facility, HMGU) or NEMO/IKK γ (FL-419, 1.5 μg) and samples were incubated in an overhead rotator overnight at 4°C . After antibody incubation, 18 μl rec-Protein G Sepharose 4B beads (1:1 suspension, life technologies) was added and lysates were rotated for an additional 1–2 h at 4°C . For Strep-Tactin pulldowns (ST-PDs), Strep-tagged CK1 α , MALT1 or CARD11 proteins were precipitated by using 30 μl Strep-Tactin Sepharose (1:1 suspension, IBA) at 4°C overnight. After incubation with Protein G Sepharose or StrepTactin Sepharose, beads were washed four times with 500 μl ice-cold Co-IP buffer without protease inhibitors ($200 \times g$, 5 min, 4°C). The supernatant was completely removed by aspiration and approx. 15–20 μl 2x SDS loading buffer (Roti®-Load1, Carl Roth) was added to the beads. Samples were boiled at 95°C for 7 min before they were separated by SDS-PAGE and analyzed by Western Blotting.

Detection of active MALT1 using MALT1 activity based probes

MALT1 activity based probes (ABPs) were used to monitor cellular MALT1 activity. An ABP coupled to biotin (probe7: biotin-KLRSR-AOMK) was used for pulldown (PD) of active MALT1 (Eitelhuber et al., 2015). 3×10^7 cells were stimulated using P/I, washed with PBS

and lysed in 600 μ l Co-IP buffer without protease inhibitors. Lysates were incubated for 20 min in an overhead rotator before samples were cleared by centrifugation (14 000 rpm, 15 min, 4°C). 30 μ l supernatant was collected as lysate control and was mixed with 4x SDS loading buffer (Roti®-Load1, Roth) and boiled for 5 min at 95°C. The residual supernatant was pre-cleared using 12 μ l High Capacity Streptavidin Beads (Thermo Fisher) for 1 h at 4°C. Subsequently, 0.1 μ M ABP probe 7 was added to the residual supernatant and incubated for 1 h at RT. To precipitate the active MALT1, 15 μ l High Capacity Streptavidin Beads (Thermo Fisher) were added for 1 h at 4°C and afterward washed four times with 500 μ l ice-cold Co-IP buffer without protease inhibitors (200x g, 5 min, 4°C). The supernatant was completely removed by aspiration and approx. 15 – 20 μ l 2x SDS loading buffer (Roti®-Load1, Carl Roth) was added to the beads. Samples were boiled at 95°C for 7 min before they were separated by SDS-PAGE and analyzed by Western Blotting.

Generation of anti-MALT1 S562, S649 and S803 phospho-specific antibodies

Monoclonal antibodies against MALT1 phosphorylation sites were generated by immunization of C57BL/6 mice and Lou/c rats with ovalbumin-coupled peptides comprising phosphorylated serine S562, S649 or S803 (S562: EYSAEpSLVRNL, S649: GSYLVpSKDLPK, S803: DEIPFPpSFSDRL). Animals were injected subcutaneously and intraperitoneally with a mixture of 40 μ g peptides, 5 nmol CpG (Tib Molbiol, Berlin, Germany) and an equal volume of incomplete Freund's adjuvant. A booster immunization was performed 6 weeks later without Freund's adjuvant and spleen cells were fused with P3X63Ag8.653 myeloma cells using standard procedures. Hybridoma supernatants were screened in a solid-phase enzyme-linked immunosorbent assay (ELISA) for binding to the respective phosphopeptides. Specificity was confirmed by negative screening on respective non-phosphorylated peptides. Positive supernatants were further validated by western blot analysis. Hybridoma cells from selected supernatants were subcloned at least twice by limiting dilution to obtain stable monoclonal cell clones recognizing phosphorylated serines pS562 (clone 24E9; rat IgG2b/k), pS649 (clone 29E12; mouse IgG2a/k) and pS803 (clone 24A4; rat IgG2c/k). Experiments were performed with hybridoma supernatant.

Western Blotting

Proteins were transferred onto PVDF-membranes for immunodetection using electrophoretic semi-dry transfer system. After transfer, membranes were blocked with 3% BSA or 5% milk for 1 h at RT and incubated with specific primary antibody (dilution 1:1000 in 3% BSA/PBS-T or 5% milk/PBS-T) overnight at 4°C. Membranes were washed in PBS-T before addition of HRP-coupled secondary antibodies (1:7000 in 1.5% BSA or 2.5% milk in PBS-T; 1 h, RT). HRP was detected by enhanced chemiluminescence (ECL) using the LumiGlo reagent (Cell Signaling Technologies) according to manufacturer's instructions.

Electrophoretic mobility shift assay

For electrophoretic mobility shift assays (EMSA), double-stranded NF- κ B or OCT1 binding sequences (H2K fw – 5' GATCC AGGGCTGGGGATTCCCCATCTCCACAGG, H2K rev – 5' GATCCCTGTGGAGATGGGGAATCCCCAGCCCTG, OCT fw – 5' GATC TGTCGAATGCAAATCACTAGAA, OCT rev – 5' GATCTTCTAGTGATTGCATTCGACA) were labeled with [α -³²P] dATP using Klenow Fragment (NEB). To monitor DNA binding, whole cell lysates (3–6 μ g) were incubated for 30 min at RT with shift-buffer (HEPES pH 7.9 (20 mM), KCl (120 mM), Ficoll (4%)), DTT (5 mM), BSA (10 μ g) and poly-dI-dC (2 μ g, Roche) and radioactive probe (10000–20000 cpm). Samples were separated on a 5% polyacrylamide gel in TBE buffer, vacuum-dried and exposed to autoradiography. Images have been cropped for presentation.

NF- κ B luciferase and EGFP reporter assays

Jurkat T cells reconstituted with empty vector (mock), CK1 α WT or D136N mutant were transfected by electroporation with a 6x NF- κ B reporter plasmid (expressing Firefly luciferase) as well as a pTKluc plasmid (expressing Renilla luciferase) (220 V, 1000 μ F, 0.4 cm cuvettes). 72 h after transfection, 2x 10⁶ cells were stimulated for 5 h with P/I or anti-CD3/CD28 antibodies and lysed in 100 μ l passive lysis buffer (PLB, Promega). A dual luciferase assay (Promega) was performed according to the manufacturer's protocol and luciferase activity was determined using a luminometer (LB 960, Berthold).

CARD11-deficient line JPM50.6 expressing the NF- κ B-EGFP reporter (Wang et al., 2002) were lentivirally transduced with pHAGE-h Δ CD2-T2A-CARD11 and pHAGE-h Δ CD2-T2A-CARD11 S608A. 7 days after transduction, infection efficiency was determined by analyzing h Δ CD2 expression and by checking CARD11 expression levels in WB. To analyze NF- κ B activity, 0.5x10⁵ cells were stimulated for 5 h with P/I. Afterward, cells were washed with PBS, taken up in 300 μ l PBS and NF- κ B activity was visualized via EGFP expression on an Attune Acoustic Focusing Cytometer.

Production and purification of recombinant proteins

N-terminally GST-tagged MALT1 325–760 was expressed in *E. coli* BL21-CodonPlus (DE3)-RIPL cells and purified via affinity chromatography using GSTrap High Performance columns (GE Healthcare). Bacteria were grown in LB-medium at 37°C with 100 μ g/ μ l ampicillin and 25 μ g/mL chloramphenicol to an OD600 of 0.6–0.8, then moved to 18°C and rotated for an additional 30 min before induction with 50 μ M IPTG. Protein was produced overnight (18°C, 150 rpm). Cells were harvested and resuspended in 7 mL of lysis buffer (50 mM HEPES pH 7.5, 10% (v/v) glycerol, 0.1% (v/v) Triton X-100, 150 mM NaCl, 2 mM MgCl₂ x 6H₂O, 1 mM DTT, protease inhibitor cocktail (Roche)). The cell suspension was lysed by sonication and subsequently centrifuged for 30 min (16,500 rpm, 4°C).

The supernatant was transferred to a new tube, and centrifugation was repeated for 60 min. The Supernatant containing recombinant MALT1 protein was applied to the ÄKTA and unspecifically bound proteins were washed through the column with wash buffer (50 mM Tris, 150 mM NaCl, pH 8.0). MALT1 was eluted with elution buffer (wash buffer with 15 mM glutathione). The eluate was concentrated to 600–800 μ L using Amicon cellulose membrane filters (Merck) and protein concentration was determined using a NanoDrop (Thermo Fisher).

Generation of MALT1 protein using the baculoviral expression system

His₆-tagged MALT1 (aa 334–824)-HA was expressed in Sf9 cells using the baculovirus expression system (Sun et al., 2004). The protein was purified using nickel affinity chromatography (Ni-NTA agarose) according to the manufacturer's instructions (QIAGEN).

In vitro kinase assay

150 ng recombinant CK1 α (Sigma-Aldrich) was incubated with 5 μ g bacterial produced and purified GST-MALT1 (aa 325–760) or 5 μ g baculoviral produced and purified 6xHis-MALT1-GyrB-HA (aa 334–824). Proteins were added into 20 μ l kinase assay buffer (25 mM MOPS (pH 7.2), 12.5 mM glycerol-2-phosphoate, 25 mM MgCl₂, 5 mM EGTA and 2 mM EDTA. Immediately prior to use, DTT was added to a final concentration of 0.25 mM). An ATP-containing assay cocktail was simultaneously prepared according to the manufacturer's guide, and 5 μ l of this mix was added to the samples. In this approach non-radioactive ATP was used. The reaction mixture was incubated for 2 h at 30°C, then 4x SDS loading buffer was added and the samples boiled for 5 min. 10 μ l sample was loaded onto a 12.5% SDS-PAGE. Phosphorylation of MALT1 on S562 was detected using the specific anti-pS562 antibody in Western Blot.

Sample preparation for phospho-peptide analyses of MALT1

For mass spectrometric analyses, Jurkat T cells were stimulated and MALT1 was enriched by ST-PD against MALT1 as described earlier. The eluates were diluted to 200 μ l with ABC buffer (50 mM ammonium bicarbonate) and digested by a modified filter aided sample preparation (FASP) method (Wiśniewski et al., 2009) as described in Grosche et al. (2016). Briefly, samples were reduced with 20 μ l DTT (100 mM) for 30 min at RT (shaking), followed by alkylation of cysteine residues with 50 μ l Iodoacetamide (300 mM) for 30 min at RT in the dark. Urea buffer (8 M Urea/0.1 M Tris/HCl (pH 8.5)) was added to a final concentration of \geq 4 M and samples were loaded onto a 30 kDa cut-off filter (Nanosep 30k OMEGA, Pall Life Sciences, Ann Arbor), that had been previously equilibrated with 200 μ l UA buffer, and centrifuged at 14,000 g for 15–30 min. After sample loading, filters were washed three times with 200 μ l urea buffer and twice with 100 μ l ABC buffer. Digestion was performed with 2 μ g Lys-C (Wako Chemicals, Neuss) in 70 μ l ABC buffer containing phosphatase inhibitors (Phosphatase Inhibitor Cocktails 2 & 3, 1:100 (v/v), Sigma-Aldrich) for 2 h at RT followed by tryptic (5 μ g, Sigma-Aldrich) digest at 37°C for 16 h. Digested peptides were collected by centrifugation at 16,000 g for 15 min and residual peptides were eluted from the filters with 20 μ l 50 mM ABC/2% ACN. Combined eluates were concentrated to 40–50 μ l in a vacuum centrifuge (Univapo 150 ECH, UniEquip, Martinsried).

For phospho-peptide enrichment, TiO₂ beads (Sachtopore NP, 5 μ m, 300Å (SNX030S005), Sachtleben Chemie, Duisburg) were resuspended in water at 125 μ g/ μ l, and 20 μ l per sample was washed sequentially with 400 μ l water, 400 μ l ACN and equilibrated in 400 μ l washing buffer (60% ACN/4% TFA) by centrifugation at 15,000 g for 1 min. The peptide eluates were diluted with 160 μ l loading buffer (80% ACN/5% TFA) and incubated with the bead preparation for 90 min at RT (shaking). The supernatant containing unbound peptides was discarded after centrifugation and the beads were washed three times for 2 min at RT with 200 μ l 50% ACN/0.1% TFA. Enriched phospho-peptides were then eluted twice with 20 μ l NH₄OH (10%) for 10 min at RT (shaking) by centrifugation (21,000 g, 3min) and the combined eluates were acidified with TFA to pH 2.

LC-MS/MS data acquisition

Enriched phospho-peptides were analyzed on an Ultimate 3000 nano HPLC system (Dionex, Sunnyvale, CA) coupled to a LTQ Orbitrap XL mass spectrometer (Thermo Fisher Scientific), equipped with a nano-ESI source.

20 μ l of each enriched sample was injected automatically and peptides were loaded onto a nano trap column (5 mm x 300 μ m i.d., packed with 5 μ m Acclaim PepMap100 C18 resin, 100 Å pore size (LC Packings, Sunnyvale)) at a flow rate of 30 μ l/min using 7% ACN/0.1% FA (v/v) in HPLC-grade water for 5 min. Separation of peptides was performed on a reversed-phase analytical column (15 cm x 75 μ m i.d., Acclaim PepMap C18 resin, 3 μ m, 100 Å pore size (Dionex)) at a constant temperature of 40°C and peptides were eluted using the following gradient conditions at a flow rate of 300 nl/min: linear from 7% ACN to 32% ACN over 60 min, linear from 32% ACN to 93% ACN in 1 min and isocratic at 93% ACN for 5 min, followed by an equilibration step for 15 min at starting conditions (all ACN buffers included 0.1% (v/v) FA).

Ionization of peptides was performed in a nano-ESI source using 1.51 kV spray voltage and a capillary temperature of 200°C. The mass spectrometer was operated in data-dependent acquisition mode, and up to the ten most intense precursor ions were selected for fragmentation. The signal of polysiloxan ($m/z = 445.12002$) was used as lock mass for internal calibration. Full scan MS spectra were acquired in the Orbitrap mass analyzer within an m/z range from 300 to 1500 with a resolution of 60,000 at m/z 400. The AGC target value for precursor ions was set to 1e6 and ions were collected up to a maximum of 500 ms. Up to ten precursors with a charge state of \geq 2 were isolated in a window of 2 Th and selected for fragmentation by CID in the linear ion trap if a minimal ion count of 200 was exceeded. Precursor ions were fragmented with 35% normalized collision energy and an activation time of 30 ms. MS/MS scans

were acquired with a resolution of 15,000 at m/z 400 and an AGC target value of $1e4$ with a maximal injection time of 100 ms. After MS/MS analysis, precursor ions were dynamically excluded for 30 s.

Mass spectrometric raw data processing and analyses

Mass spectrometric raw data was analyzed with Proteome Discoverer Software (Version 1.4.1.14, Thermo Fisher Scientific) using Mascot (Version 2.5.1, Matrix Science, London) as a search engine. MS/MS spectra were searched against Ensembl Human database (Release 80, May 2015) with a precursor mass tolerance of 7 ppm and a fragment mass tolerance of 0.7 Da, carbamidomethylation (C) as static modification, and deamidation (N,Q), oxidation (M) and phosphorylation (S, T, Y) as dynamic modifications. Enzyme specificity was set to trypsin and up to two missed cleavages were allowed. For the confident localization of phospho-sites, the phosphoRS (Version 3.0) node was included in the Proteome Discoverer workflow. MALT1 identifications were adjusted to $< 1\%$ FDR at PSM level based on Percolator q-Value.

QUANTIFICATION AND STATISTICAL ANALYSES

For statistics all experiments in CD4 and Jurkat T cells contained at least four biological replicates and values represent the mean \pm standard deviation (SD). Experiments were analyzed by using unpaired Student's t test. Statistical significance p values are: * $p < 0.05$, ** $p < 0.01$, *** $p < 0.001$, **** $p < 0.0001$. For statistics of DLBCL cell growth, error bars depict standard errors of the mean (SEM) over 4 biological replicates for each time point and vector. For each time point, we first computed the ratio $r_{VtoNoV} = n_V/n_{NoV}$ of living cells having the vector (n_V) to living cells not having the vector (n_{NoV}) from the measured ratio r_{VL} of cells having the vector in the subset of all living cells. As $n_V+n_{NoV} = n_{AllLiving}$, i.e., 100% with respect to the scale of r_{VL} , we have $n_V/n_{NoV} = r_{VL}/(1-r_{VL})$. Second, for each two-days-interval between two measured time points, we then computed the relative cell growth or dying rates of with versus without vector: $rescueRate = r_{VtoNoV}(t+2days)/r_{VtoNoV}(t)$. If rescuing takes place in a given 2-day time interval, cells with the vector will grow faster or die slower than cells without the vector, i.e., the rescue rate will be $> 100\%$ for this time interval. As these rescue rates are multiplicatively defined, we \log_2 -transformed them to obtain normally distributed values: $l2rescueRate = \log_2(rescueRate)$. To determine the rescue effects that are consistent over time versus the MALT1 WT vector, we finally compared $l2rescueRate$ (for a given MALT1 mutant vector) with $l2rescueRate$ (for MALT1 WT) via t tests (paired over time points, one-tailed). Notably, these paired comparisons automatically normalize for any vector-independent effects on cell growth/death rates that affect both compared vectors and are shown by the empty vector curve.

DATA AND CODE AVAILABILITY

The published article includes all data generated or analyzed during this study. Original source data for Figures in the paper are available upon request to the Lead Contact author. No proprietary software was used in the data analysis.